

Detection systems for mass spectrometry imaging: A perspective on novel developments with a focus on active pixel detectors

Julia H. Jungmann and Ron M. A. Heeren*

FOM Institute AMOLF, Science Park 104, 1098 XG Amsterdam, The Netherlands

Instrumental developments for imaging and individual particle detection for biomolecular mass spectrometry (imaging) and fundamental atomic and molecular physics studies are reviewed. Ion-counting detectors, array detection systems and high mass detectors for mass spectrometry (imaging) are treated. State-of-the-art detection systems for multi-dimensional ion, electron and photon detection are highlighted. Their application and performance in three different imaging modes – integrated, selected and spectral image detection – are described. Electro-optical and microchannel-plate-based systems are contrasted. The analytical capabilities of solid-state pixel detectors – both charge coupled device (CCD) and complementary metal oxide semiconductor (CMOS) chips – are introduced. The Medipix/Timepix detector family is described as an example of a CMOS hybrid active pixel sensor. Alternative imaging methods for particle detection and their potential for future applications are investigated. Copyright © 2012 John Wiley & Sons, Ltd.

1. INTRODUCTION TO SENSORS AND DETECTORS

Webster's New World Dictionary defines a sensor as a "device to detect, measure, or record physical phenomena (...)"^[1] However, the definition of what exactly distinguishes a sensor from a detector is often not clear cut and the concepts 'sensor', 'detector', 'sensor system' and 'detector system' are used interchangeably in the literature. The part of the system that actually 'interacts' with the parameter of interest and transforms it into a measurable quantity is generally referred to as a transducer. Hence, transducers are part of a more complex sensor/detector system. The sensor or detector measures the 'transduced' parameter and converts it into an electrical signal which can be read by an instrument or user.

Measurement instruments are deeply engrained into our daily lives. Many of us cannot imagine living without fever thermometers, motion-sensors, central heating thermostats, television remote controls, digital photo cameras, medical imaging equipment for X-ray absorption and computed tomography scans, to name only a few examples.

Many of those 'daily life' sensor and detection systems were originally developed for scientific research. Only later were they spun-off as user products. Applied and fundamental physics research are active areas of sensor and detector instrumentation development. In these disciplines, dedicated systems are developed for a specific experiment or application field. In this way, the detection system is maximally sensitive to the parameter of interest.

The development of instrumentation for imaging and individual particle detection has progressed tremendously over the past decades. In biomolecular mass spectrometry

imaging and fundamental atomic and molecular physics studies, such detection systems register ions, electrons and photons among other particles. The (charged) particle detectors in these fields are mainly instruments that detect, identify or track particles. They measure such quantities as the particle energy, the impact position, the particle charge, and the intensity of particles. The state-of-the-art ion, electron and photon detection and imaging technology, specifically applied in the areas of mass spectrometry (MS), mass spectrometry imaging (MSI) and atomic and molecular physics research, will be introduced in this article.

2. SELECTED SENSOR AND DETECTOR TECHNOLOGY FOR MASS SPECTROMETRY

This section highlights two examples of the most important detection systems employed for the detection of charged particles in mass spectrometers. It does not attempt to give an in-detail, historic overview of mass spectrometry detectors, rather it emphasizes a few detection systems which are in frequent use in mass spectrometry today and/or are potential detection systems for MSI.

2.1. Array detectors

Array detectors are traditionally used to record the spatial distribution of a variety of particles, ranging from photons, to sub-atomic particles, atoms and ions. In mass spectrometry, array detectors are used for the simultaneous detection of multiple ions of different mass-to-charge ratio (m/z values). Hence, detector arrays improve the detection limits and measurement precision.^[2,3] They reduce the sample consumption and increase the instrument's duty cycle.^[2,3] Array detectors are a particularly interesting group of detection systems since they are relevant both to MS and to MSI research.

* Correspondence to: R. M. A. Heeren, FOM Institute AMOLF, Science Park 104, 1098 XG Amsterdam, The Netherlands. E-mail: heeren@amolf.nl

2.1.1. Microchannel plate detectors

A microchannel plate (MCP)^[4] is a thinly sliced plate that consists of several millions of parallel, small diameter, conductive glass tubes which have been fused together. Typical pore diameters are 10 to 100 μm and the channel length-to-diameter ratios are 1:40 to 1:100. The channel axes typically assume a small angle ($< 10^\circ$) with respect to the normal to the MCP surface to enhance primary particle detection. A bias voltage is applied across the plate(s). When a primary particle hits the wall of a MCP channel, it liberates secondary electrons. Similar to the working mechanism of a photomultiplier, these electrons free more electrons in turn. Each channel works as an independent secondary electron multiplier. Figure 1 shows a schematic representation of an MCP.

A single MCP typically has a gain of 10^4 . When higher gains are used, instability and 'ion feedback' are observed, i.e. atoms inside the channels are ionized and travel in the opposite direction to the electron avalanche. For higher gains, MCPs are typically arranged in a chevron stack of two plates or a Z-stack of three plates, which translate a single ionizing particle at the front side of the MCP into a multi-million electron shower (gains $>10^6$) at the back side of the MCP stack. MCPs have a fill factor, i.e. the ratio of the open pore area to the total MCP area, of about 70 to 80%. As a result, any detection system in combination with a MCP cannot reach unit detection efficiency. However, it is advantageous if the second detector stage is capable of registering the full particle load exiting the MCP.

Many detection systems for both mass spectrometry (MS) and mass spectrometry imaging (MSI) are based on MCPs. The MCP is used as a conversion/amplification medium^[4] which translates a single ion event into a measurable signal. MCPs can be sensitive to electrons, ions, photons (in the ultraviolet (UV) and soft X-rays) and neutrons (possibly in combination with an enhancing coating), etc.

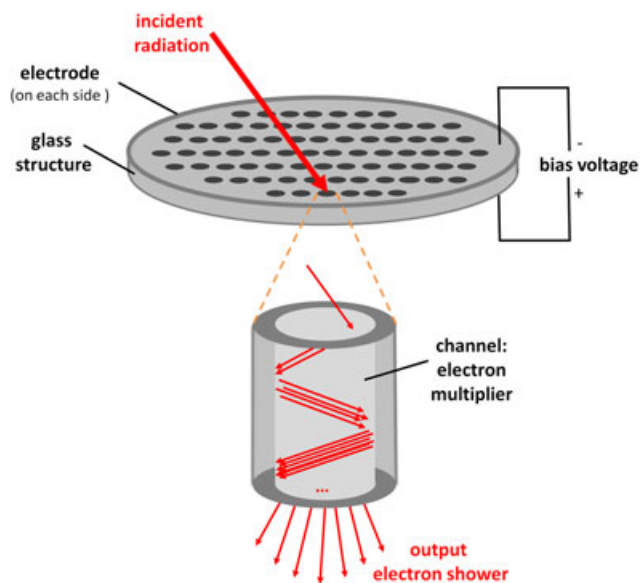


Figure 1. Schematic representation of a microchannel plate. A chevron or a Z-stack of MCPs consists of two or three such plates, respectively. The dimensions of the output electron shower depend on the MCP bias voltage (i.e. the gain of the plates), the channel diameter and length, the channel bias angle and the distance between the back side of the MCP and the electron-receiving detection system.^[5]

Due to their fast response, MCPs can be used for time-of-flight (TOF)-MS measurements in combination with a time-to-digital converter (TDC) where timing resolutions on the order of tens of picoseconds have been realized.^[6] In addition, the large MCP area enables the integration of many counts on the detection system. However, MCPs are also often used in combination with a second detector system, both for MS and MSI. Examples include electro-optical imaging detectors (section 3.2.1.) and charge-division detectors (section 3.2.2.). These detection systems are also used in MSI and are therefore treated in section 3. In MS research, MCPs have also been combined with capacitively coupled detectors and discrete-anode array detectors, which are not covered here.

As with other detection systems which rely on translating particle momentum into a particle count, a limitation of MCPs in MS is the so-called 'high-mass roll-off' of the detector. In a MCP, the ion detection depends on the generation of secondary electrons. The generation of a secondary electron avalanche is proportional to the velocity of the incoming particle. As all particles in a TOF mass spectrometer are theoretically given the same kinetic energy, high-mass ions will impinge on the detector with a relatively low velocity/momentum. Hence, they deposit insufficient energy to create an electron shower. Thus, the high-mass ions are not detected. The limitations associated with MCPs in imaging experiments are covered in section 3.2.4. Detection systems for high mass ions are described in section 2.2.

MCPs are often used as an amplification/conversion stage in the detection process. They are then combined with a second detector stage. Such combinations are mainly used in imaging applications and are covered in section 3.2. MCPs are generally well understood and characterized detectors. They are not covered in further detail here. The interested reader is referred to references^[2,4] which cite some 20 publications that document the characterization of MCPs and their performance under several experimental conditions.

2.2. High-mass detection systems

This section highlights selected high-mass detection systems for MS. In particular, the Covalx HM high-mass detection system for macromolecules up to 1.2 MDa is described. In addition, cryogenic detectors based on superconducting tunnel junctions, calorimeters/bolometers and recently developed superconducting nanostripline detectors/nanomembrane detectors are introduced.

2.2.1. The Covalx HM high-mass detection system

The Covalx HM high-mass detection system (Covalx, Zurich, Switzerland) provides an alternative detection method that circumvents the high-mass roll-off.^[7,8] The Covalx HM system uses conversion dynode technology, which enables the detection of macromolecules up to 1.2 MDa at nano-molar sensitivity. This ion conversion detector system increases the sensitivity for the detection of higher mass ions by colliding the ions of interest with a conversion dynode array. The conversion dynode transforms the initial (macromolecular) ions into smaller 'secondary' ions, which are accelerated towards a secondary electron multiplier. Due to their higher velocity, the accelerated 'secondary' ions are detected with a higher sensitivity than the initial ions would be. Van Remoortere

and co-workers have employed the Covalx HM system for matrix-assisted laser desorption/ionization (MALDI)-TOF MSI and profiling of proteins from tissue, of up to 70 kDa and 110 kDa in mass, respectively.^[8] Seyfried and co-workers employed the Covalx HM detector on a liner MALDI-TOF MS instrument for the analysis of PEGylated (glyco)proteins in the mass range of 60–600 kDa.^[9] They compared the performance of the Covalx to a standard secondary electron multiplier (SEM) detection system. They concluded that the Covalx HM shows significantly better performance in the mass range above 100 kDa, while the standard SEM outperforms the Covalx HM for protein analysis in the low-mass range due to a better signal-to-noise ratio.

2.2.2. Cryogenic/bolometric detectors for high-mass ion detection

Cryogenic detectors^[10–13] involve a detection mechanism at low, sub-Kelvin, temperatures. Cryodetectors are particularly useful for the detection of high-mass (hundreds of kDa) macromolecules, which cannot be registered with most other detection systems such as, for instance, MCPs, due to the detector roll-off at high masses. In a TOF mass spectrometer, all ions are given the same kinetic energy of the order of 5–30 keV. Due to their high mass, macromolecular ions impinge on the detector with a relatively low velocity/momentum. They remain 'unseen' by most detection systems since they do not liberate sufficient charge carriers within the detection medium. Cryogenic detection systems have a mass-independent response. They detect slow-moving particles with near-unity efficiency. In addition, they not only detect the arrival of the ion on the detector, but also measure the energy deposited by the impinging biomolecular ion. The kinetic energy of the ion is directly proportional to its charge state z . Therefore, the energy measurement can be used to identify the charge state of the ion. This is particularly interesting in TOF-MS, where the TOF is proportional to the mass-to-charge ratio, m/z value, of the ion. Hence, the singly charged monomer, doubly charged dimer and triply charged trimer, etc., have the same m/z value and they cannot be distinguished solely by their TOF.

One type of cryogenic detector is superconducting tunnel junctions. In this system, charge carriers (quasi-particles) are excited across a meV energy gap similar to electron-hole pair generation in a semiconductor material. The current of charge carriers is registered as the arrival signal. The number of created excitations is proportional to the absorbed energy. The macromizer (Comet AG, Flamatt, Switzerland) is a commercial cryogenic detection system based on superconducting tunnel junctions. Zenobi and co-workers have demonstrated the analysis of megadalton compounds (>500 kDa) on a MALDI-TOF mass spectrometer using the macromizer.^[14] The molecular protein characterization of human plasma lipoproteins using the macromizer was shown by Heller and co-workers.^[15]

Another type of cryodetectors is calorimeters and bolometers based on superconducting thermometers. In these detection systems the macromolecular ion is received in an absorber material. The kinetic energy of a particle is converted into an increase in temperature, which is measured by a temperature transducer. Similarly to superconducting tunnel junctions, the arrival of high-mass ions is registered and their kinetic energy is measured.

Recently, high-mass ion detection has been demonstrated with superconducting nanostripline detectors (SSLDs).^[16,17] These detection systems comprise a number of narrow (hundreds of nanometers), thin (few nanometers) superconducting Niobium nanowires arranged in a parallel configuration. Zen and co-workers have demonstrated the detection of macromolecules up to 132 kDa with such a detection system.^[16] Advantages of the SSLDs are the sub-nanosecond response time (compared with several tens of nanoseconds in superconducting tunnel junctions) and the relatively higher operational temperature of 4.2 K instead of 0.3 K.

Another novel development for high-mass ion detection is mechanical nanomembrane detectors for TOF MS.^[18] These detection systems consist of a nanomembrane, an extraction electrode, a microchannel plate (MCP) and an anode. Ion impacts excite mechanical vibrations in the nanomembrane. These oscillations are detected on the MCP/anode by time-dependent field emission of electrons from the vibrating membrane. MALDI-TOF MS on proteins up to 150 kDa has been demonstrated with this system.

2.3. Mass spectrometry + imaging

In mass spectrometry, array detectors^[2,3] have the capability to simultaneously detect multiple ions of different m/z values. This has the advantages of increasing the detection limits and the measurement precision, and it increases the duty cycle of the instrument.^[2]

In addition to these advantages, sample-correlated, position-sensitive detection can introduce another dimension of experimental information to a mass spectrometric measurement. In particular, MSI merges the benefits of analyte identification by MS with the localization information from projecting sample analytes onto a position-sensitive detector. In this way, MSI provides the capability to identify analytes of interest and localize them in the 'context' of their functionality on a sample surface. Many techniques have been developed for MSI.^[19,20] Position-sensitive detector technology dedicated to MSI (and related techniques) is treated in section 3.

3. STATE-OF-THE-ART IN MULTI-DIMENSIONAL ION, ELECTRON, PHOTON IMAGING AND DETECTION IN MSI, ATOMIC AND MOLECULAR PHYSICS AND RELATED AREAS

3.1. Different modes of imaging and particle detection

It is important to distinguish between different modes of imaging and particle detection since every application has its distinct requirements on what information is to be extracted from the detection of the ions, electrons, or photons. The information recorded in the different imaging/detection modes differs significantly, although all modes rely on the detection of individual particle events. Figure 2 gives an overview of the different modes of detection.

(1) Integrated image detection

Imaging typically involves the (untriggered) accumulation of particle counts on the detector or the integration of particle counts from multiple image acquisitions. The acquired image

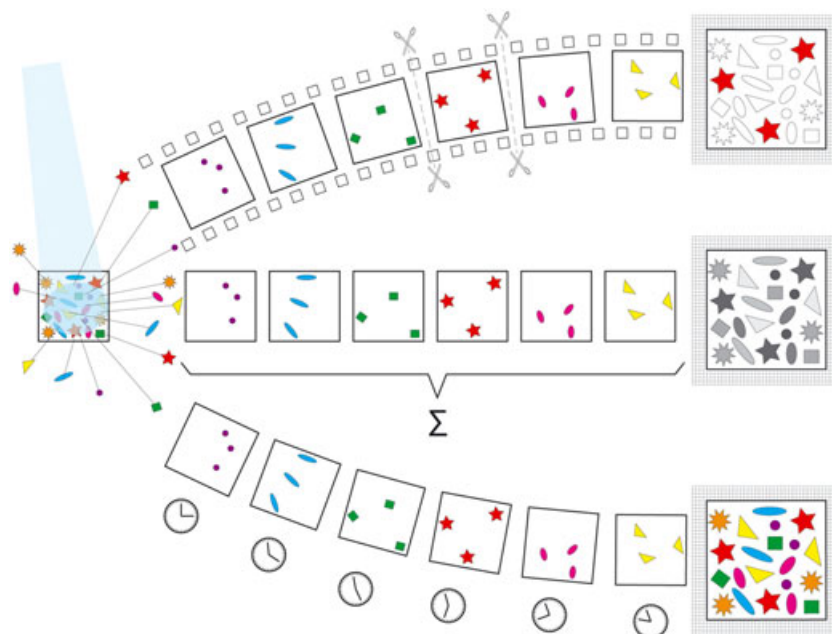


Figure 2. Overview of the three different modes of imaging and particle detection: integrated image detection, selected image detection, and spectral image detection. The differences between the three imaging modes are illustrated with the example of TOF MS imaging. On the left-hand side, the sample is ablated with a surface probe, and ions are generated. The ions are sent through the TOF mass spectrometer, in which they are mass separated. Different mass ions travel behind one another as ‘molecular images’. In integrated image detection (middle), the total ion current is received on the imaging detector. Different masses cannot be distinguished in the image. In selected image detection (top), part of the ion cloud is selected and the localization of this particular mass on the imaging detector is registered. In spectral image detection (bottom), the detection system precisely registers the arrival time and the arrival position of each mass.

gives information on the spatial distribution of the particles. The intensity distribution of registered events provides detail on the relative quantity of particles.

Medical X-ray or computed tomography (CT) imaging relies on this type of image acquisition. A ‘total ion image’ in MSI, i.e. an image of the full ion current, is also accumulated in this way. In addition to the particle intensity, other quantities such as, for instance, the particle velocity, momentum or energy, may be extracted from such images in dedicated experiments in which the specific projection method and reconstruction algorithm allow the correlation of image features with these quantities. An example of such a technique is velocity map imaging (VMI)^[21,22] which is employed in fundamental atomic and molecular physics studies. Another example is a laser beam profile measurement where the spatial distribution of the beam intensity is measured with a position-sensitive detector. Hyperspectral imaging is another technique that makes use of integrated image detection, where objects are investigated by illuminating them with a wide range of optical wavelengths. Depending on its composition, the object under investigation reflects these wavelengths in a characteristic way such that a position-sensitive sensor records a spectroscopic signature of several spectral bands.

(2) Selected image detection

A specific, selected part of an event distribution is imaged by gating the detection system or by deflecting particles from reaching the detector, i.e. part of the ‘spectrum’ of information is collected. In this imaging method, the particle selection or detector gating is triggered with respect to the origin of the event creation.

For example, it is desirable to image a selected part of an event distribution in microscope mode MSI.^[23] Here, the total ion current can be measured without m/z -specific localization on the sample during one acquisition (‘integrated image detection’ as described in (1)). Or, alternatively, a particular m/z species can be selected to pass to the detector by a pair of fast-switching electrodes. The combination of several mass-selected images from separate measurements then gives information on the sample composition and the according spatial distribution. This detection approach allows the successive localization of selected m/z species. However, it bears the disadvantage of time-consuming, highly repetitive measurements having to be made on quickly depleting biological samples.

Another example of gated imaging is ‘slice imaging’,^[24–26] a variant of VMI. In slice imaging, the detection is restricted to particles with a specific time-of-flight by rapidly gating

the detector. This allows one to exclude all particles from the measurement that have a non-zero velocity component perpendicular to the detector plane, i.e. this method images the 'center slice' of the reaction sphere. By measuring the ion distribution of interest directly, slice imaging does not require a mathematical reconstruction of this distribution from the total ion distribution. Therefore, slice imaging is a time-efficient and convenient alternative to VMI.

(3) Spectral image detection

The detection of individual particles typically involves the triggered and precise registration of the particle's impact position and its arrival time. Time-of-flight mass spectrometry imaging identifies ions by measuring the individual ion's TOF with respect to an external trigger and localizes them by registering their position on the detector. The time- and position-sensitive detection of individual ions enables the identification and localization of the full ion load in one experiment (contrary to the (gated) imaging described in (1) and (2)) at sufficiently low count rates.

In fundamental atomic and molecular physics research, cold target recoil ion momentum spectroscopy (COLTRIMS) in 'reaction microscopes'^[27-29] measures the vector momenta of several ions and electrons from an induced atomic or molecular reaction coincidentally. A combination of electric and magnetic fields guides all emitted ions and electrons to opposite time- and position-sensitive detectors. The position of impact, the TOF and the measurement geometry enable the reconstruction of the particles' trajectories and the reconstruction of their initial momenta, which enables fundamental insight into the nature of these reactions.

The imaging atom probe is the imaging variant of the atom probe field ion microscope.^[30,31] In an imaging atom probe setup, a position- and time-sensitive detector is placed at a distance of several centimeters from the tip. The detection system identifies the sample particles from the tip by TOF MS. The imaging ion probe also provides information on the localization of the analytes within the sample by projecting the particles onto the position-sensitive detector while retaining the spatial information from the sample surface. Specifically, the imaging atom probe is used to identify different species and their distribution on a crystal surface. Note that early imaging atom probes were operated in detector gating mode (as described in (2)). The identification and localization of individual particles on the atom probe tip provide the possibility of depth profiling and three-dimensional sample reconstruction, i.e. atom-probe tomography.

The choice of detection system and imaging/detection method largely depends on the mode of imaging or particle detection that a particular application requires. In addition, considerations such as the measurement conditions (gas pressure, temperature, chemical environment, etc.), practicability and system handling may play a significant role in the choice of detection system (see section 3.3, performance criteria).

3.2. State-of-the art imaging/particle detection systems

State-of-the art particle imaging and detection systems currently include electro-optical image detectors, i.e. microchannel plates (MCPs) in combination with a photon detector. In addition, there are charge division detectors such as MCP detectors

in combination with a resistive anode, delay-line detector (DLD), a shaped or a cross-strip anode (XSA), or a hybrid active pixel detector (HAPS). Hybrid active pixel detectors are often combined with a semiconductor sensor layer or a gaseous particle conversion medium. Therefore, they do not necessarily require an MCP for sufficiently high energy particles (see section 5).

For imaging applications, the spatial resolution obtainable with an MCP is particularly relevant. Here, it should be noted that the spatial resolution in such a detector depends on the spread of the electron cloud exiting the back side of the MCP, and if applicable the element size of the detection system. The dimensions of this electron cloud depend on the distance between the back side of the MCP and the secondary detection stage, the potential between these two detection stages, the pore bias angle, and the pores size.^[5] The use of a MCP (stack) intrinsically limits the spatial resolution of the detection system due to the dimensions of the pores. In addition, the ion-electron shower conversion introduces uncertainty to the impact position information. Most electrons stay within one channel of the MCP. However, some electrons leave one channel and enter others, thereby enlarging the electron cloud. In addition, the electron shower can spread from one to several MCP pores when the electron avalanche transfers from the first, to the second and possibly third MCP plate. This effect can be partially corrected for by using centroiding algorithms. Ultra-high spatial resolution has been realized by using MCPs in combination with a segmented second detector by means of centroiding algorithms.^[32-34]

3.2.1. Electro-optical imaging detectors: MCP + photon detector

Generally, photon detectors convert the MCP electron shower into a photon signal. The electron-to-photon conversion is typically performed in a phosphor screen or a scintillation crystal. The photons are then collected by a photo-sensitive detector such as, for instance, a photo-plate,^[35] an array of photo-diodes,^[36-38] a Vidicon camera system,^[39] or a CCD camera. Electro-optical imaging detectors used for MSI are MCP-phosphor screen-CCD camera systems, which are described below. For details on the other systems, the reader is referred to the literature.^[35-39]

Phosphor screens and CCD cameras

A phosphor screen is a thin plate of phosphorus material. Different types of phosphor screens are available, which differ in their emission spectrum and their fluorescence lifetime. In a MCP-phosphor screen-CCD camera combination (Fig. 3), the electron cloud from the back side of the MCP is accelerated towards the phosphor screen, which converts the electron signal into photons. The electron-photon conversion factor depends on the phosphor material and the kinetic energy

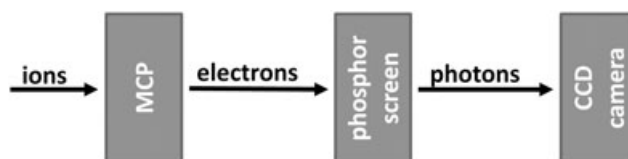


Figure 3. Schematic representation of the signal flow in a MCP, phosphor screen, CCD camera detection system.

of the electrons, and it is typically between 20 and 200 photons per electron. It is possible to coat the back side of the phosphor screen with an aluminum layer to increase the number of photons that are emitted towards the CCD camera.^[40] CCD cameras are described in detail in section 4.1 on solid-state pixel detectors.

3.2.2. MCP in combination with a charge division detector

In charge division detectors, the electron shower from the MCP is collected by an anode array, which divides the charge among several of its elements. Examples of charge division detectors are resistive anodes, delay-line anodes, shaped-anodes, cross-strip anodes and hybrid active pixel detectors.

Resistive anode encoders

A resistive anode encoder detection system,^[41–43] for secondary ion mass spectrometry, ion microscopy and other applications,^[42,43] typically consists of a chevron MCP behind which a resistive anode is mounted. When an electron cloud from the MCP hits the anode plane, a current is delivered to each corner of the anode, typically four corners. The electrodes at the corners of the anode plane are each capacitively coupled to a charge-sensitive pre-amplifier. The x- and y-positions of the event can be computed from the amount of current flowing in each of the four corner electrodes. An advantage of resistive anode encoders is the simplicity of both the detector itself and the electronics. A major disadvantage of resistive anodes is their inability to distinguish simultaneous events. Count rates in excess of 600 kHz are inaccessible. In addition, image distortions have been reported.^[41]

Delay-line detectors (DLD)

A delay-line detector is a two-dimensional (2D), position- and time-sensitive detection system. There are two different classes of delay-line systems. A crossed delay-line detector consists of two orthogonal anodes (Fig. 4). A hexanode delay-line system^[44–46] comprises three groups of two wires which are set up at a 120° angle with respect to one another.

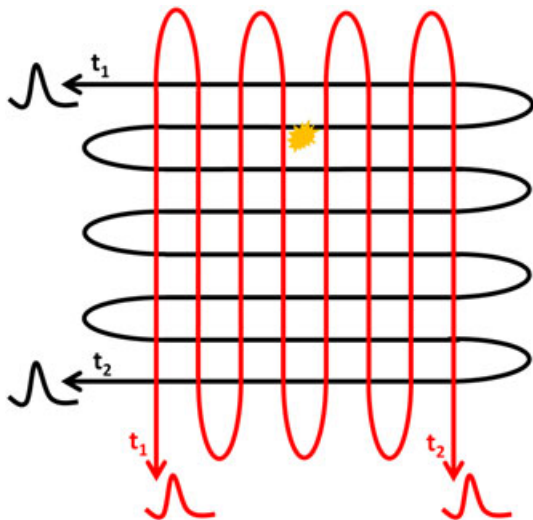


Figure 4. Schematic representation of a crossed delay line detector.

In a delay-line system, the particles which are to be detected impinge on the 2D detector plane. They induce a signal on the delay-line wires, which will travel towards both ends of the wires. The arrival of the two signal pulses at the end of the wire is registered and the difference in arrival time is measured. Since both signal pulses propagate the wire at the same speed, the difference in arrival time indicates the distance they have travelled and hence where the particle has impinged on the detector plane. In a crossed delay-line assembly, the position of particle impact is determined from two orthogonal delay-lines. Multiple (nearly) simultaneous hits cannot unambiguously be reconstructed from a two wire assembly. A hexanode delay-line system is capable of unambiguously distinguishing a few simultaneous events because the three delay-line wires introduce measurement redundancy.^[44–46] The measurement redundancy reduces the ‘dead area’ of the position-sensitive detection system after each event, which originates from dead time of the timing electronics. Often, each of the three ‘wires’ consists of a pair of wires, hence the name ‘hexanode’, in a Lecher-line configuration. Such a differential signal line provides almost background-free signals by transmitting high-frequency signals with low damping and dispersion. The pulses from the delay-lines are typically (pre-) amplified, pass a constant-fraction discriminator (CFD) and are then time-stamped by a high timing resolution, of the order of 25 ps, time-to-digital (TDC) converter. Signal reconstruction is necessary. Since the position of impact has to be retrieved from the timing measurements, the reconstruction of integrated images can be computationally involved and time-consuming particularly at high count rates.

Shaped anodes

Shaped-anode detectors provide high spatial resolution detection with a small number of individual, ‘shaped’ detector elements. The original configuration is the so-called wedge-and-strip anode (Fig. 5). The y-position is determined by wedge-shaped electrodes, which are obtained by dividing rectangular electrodes diagonally. The x-position is measured by rectangular electrodes, the ‘strips’, which vary in width across the array. All electrodes measure the deposited charge and the relative amount of charge deposited on the different wedges, and the strips indicate the central position of the MCP charge cloud. More sophisticated, simplified shaped-anode detectors have been developed.^[47,48] A spatial image resolution of better than 20 μm^[49,50] has been reported. Distinguishing simultaneous events can, however, be a problem.

Cross-strip anodes (XSA)^[51–53]

Two sets of orthogonal (‘cross’) strips are deposited on a substrate layer. The two layers of strips, the ‘x-fingers’ and the ‘y-fingers’, are separated from one another by insulating strips. The area coverage of the detection system is close to unity. The signals from the fingers are typically pre-amplified, shaped, digitized and time-stamped. When an electron cloud impinges on the fingers of an XSA, the amount of signal detected on the x- and y-fingers enables the reconstruction of the event’s impact position.

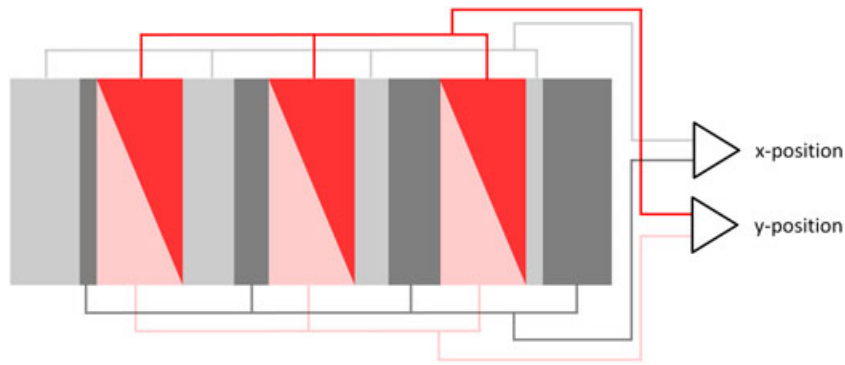


Figure 5. Wedge-and-strip anode.

Hybrid active pixel sensors

Hybrid active pixel sensors (HAPS) are pixelated image sensors which are typically composed of an application-specific integrated circuit (ASIC) and a semiconductor substrate layer. Each ASIC pixel is connected to a cell of the semiconductor layer. 'Active' pixel sensors contain much functionality on the pixel-level. In particular, each pixel has its own charge-to-voltage converter, often a (pre-) amplifier, noise corrections, discriminators or other digital signal treatment functionality. Hybrid active pixel sensors will be treated in detail in section 4.2.

3.2.3. Areas of application

Currently, MCPs in combination with crossed-delay line detectors or cross-strip anodes are used for imaging atom probe, COLTRIMS,^[29] MSI experiments,^[54,55] X-ray photoelectron spectroscopy (XPS),^[56] and Auger photoelectron spectroscopy^[57] for surface chemistry. The MCP, phosphor screen, CCD camera combination is used for microprobe mode MSI^[23] and velocity map imaging experiments.^[22,58] Pixelated detectors with a semiconductor sensor layer are used for velocity map imaging.^[59] An MCP in combination with a bare pixelated detector is used for MSI.^[60-64]

3.2.4. Performance overview of MCP-based detection systems

Table 1 gives an overview on which of the detection systems can be operated in which particle imaging/detection mode. All detection systems are capable of untriggered image acquisition by particle counting and of gated imaging. Only the MCP in combination with the phosphor screen and CCD

camera, the resistive anode encoder and the shaped anode cannot register the position and the TOF of individual particles. The state-of-the-art performance of these detection systems and their limitations are discussed below.

Vallerga, Tremsin and co-workers of the Space Science Laboratory of the University of Berkeley (Berkeley, CA, USA) have developed state-of-the-art detector technology for high spatial, high temporal resolution, high count rate detection of UV photons, electrons, neutrons and small ions. They have developed detection systems composed of a MCP stack in combination with a crossed delay line detector,^[65-68] a shaped anode,^[47] a cross-strip anode,^[34,69] and a Medipix/Timepix ASIC.^[32,71-73] Table 2 compares the performance of these systems and with those of a MCP in combination with a phosphor screen and a CCD camera,^[40] a MCP followed by a hexanode delay-line system,^[44-46] a MCP combined with a resistive anode encoder,^[41-43] and a shaped anode detector.^[47-50]

3.3. Performance criteria for detector technology

In addition to application-specific analytical performance, practical performance criteria play an important role in choosing an appropriate detection system for a particular application. Such criteria are, for instance, the available detector shape and size, the required operating environment (pressure, temperature, chemical requirements), the life time of the detection system, the required maintenance, and the ease and cost of replacement. Analytical attributes for both imaging and individual particle detection include the detector noise, the maximum event count rates, the detector

Table 1. Imaging/particle detection systems versus different imaging modes

	Integrated image detection: x,y, intensity; untriggered	Selected image detection: x,y, intensity; triggered & selective	Spectral image detection: x,y,tof; triggered
MCP + phosphor screen + CCD camera	yes	yes	no
MCP + resistive anode encoder	yes	yes	no
MCP + crossed delay-line detector	yes	yes	indirect*
MCP + hexanode delay-line detector	yes	yes	indirect*
MCP + shaped anode	yes	yes	no
MCP + cross strip anode	yes	yes	indirect*
(MCP +) hybrid active pixel sensor	yes	yes	direct

*Indirect spectral image detection via event reconstruction.

Table 2. Performance comparison between a MCP plus phosphor screen and CCD camera, resistive anode encoder, crossed delay line, hexanode delay line, shaped anode encoder, cross strip anode, and Medipix/Timepix detection system

Point of comparison	MCP + phosphor + CCD camera	MCP + resistive anode encoder	MCP + crossed delay line detector	MCP + hexanode delay line detector	MCP + shaped anode detector	MCP + cross strip anode	MCP + hybrid active pixel detector (Medipix/Timepix)
Detector	Phosphor screen, 1000 × 1000 pixels on CCD chip	4 resistive anodes	2 orthogonal wires	3 wires at 120° to one another	Matched electrodes in the shape of wedges and strips	2 × 64 orthogonal wires	256 × 256 pixels per chip
# of MCP used	2	2	3	2	2	2	1 or 2 [†]
Typical detector size	40–70 mm diameter	25 mm active area	40 mm diameter	70 mm diameter	25 mm diameter	40 mm diameter	28 × 28 mm ²
Required MCP gain	10 ⁶	10 ⁶	10 ⁷	10 ⁷	10 ⁵ –10 ⁷	10 ⁶	10 ⁴ –10 ⁵
# Amplifiers	1	4	4	6	≥ 6	128	65 k
Spatial resolution	50–200 μm	1–2 μm	~17–50 μm FWHM	13 μm	20 μm	~10 μm FWHM	- 55 μm in MPX mode - 3–5 μm FWHM in TOT mode*
Time resolution	1–33 ms [‡]	Not applicable	~130 ps – 25 ns	25 ps	Not applicable	~750 ps	~10 ns
Maximum count rate	1 MHz	600 kHz	1 MHz ^{††}	2 MHz	50 kHz	5 MHz	- GHz in MPX mode - 1 MHz at high resolution**
Noise of detector	25 electrons	electronic noise	3000 electrons	electronic noise	electronic noise	1500 electrons	100 electrons
Typical achievable vacuum	10 ⁻⁹ mbar	10 ⁻¹⁰ mbar	10 ⁻¹⁰ mbar	10 ⁻¹⁰ mbar	10 ⁻¹⁰ mbar	10 ⁻¹⁰ mbar	10 ⁻⁷ mbar

[†]A chevron MCP stack is advantageous to prevent ion feedback through the MCP pores.

^{*}In TOT mode, this resolution is achieved using a center-of-gravity centroiding algorithm. The ultimate spatial resolution is limited by the MCP pore size.

^{**}A typical cluster from the MCP spans about 5 × 5 pixels = 25 pixels on the pixel detector. Typically, about 10% of the detector's pixels are used per frame, i.e. there are about 250 events per frame (= 250 events × 25 pixels/event = 6250 pixels used of 65 k pixels). For a 2 × 2 chip assembly, there are 4 × 250 events = 1000 events per frame. The Berkeley readout runs at 1 kHz. Therefore, 1000 events/frame × 1000 frames/s = 1 million events/s = 1 MHz.

^{††}This is an exceptionally high count rate.

[‡]The time resolution is determined by the frame rate of the camera: Time resolution = 1/frame rate. Typically, frame rates are between 30 and 1000 frames/s.

dynamic range, the quantum efficiency, the detector stability and homogeneity, multi-hit capabilities, the detector response, recovery and read-out time.

Most of these performance criteria are relevant to any application. However, depending on the quantities to be measured, some performance criteria are more stringent than others. In the integrated image detection mode and in the selected image detection mode, the (reconstructed) detector element size is one of the most important performance criteria since it is directly related to the lateral image resolution. In the spectral image detection mode (x,y,TOF), both the position of impact and the TOF of the particle have to be determined precisely. In terms of detector performance this translates into fine detector segmentation for unambiguous 2D position information and high time resolution measurements and high particle count rates. The performance criteria of three detection systems are compared for microscope mode mass spectrometry imaging in Jungmann and Heeren.^[20]

4. SOLID-STATE PIXEL DETECTORS

Throughout the last decade, solid-state pixel detectors have been introduced to many areas of research and daily life. Solid-state chips are widely used in applied and fundamental (physics) research experiments as well as in daily life appliances such as hand-held digital photo cameras and mobile phones. As the wide areas of application suggest, these chips are practical and cost-efficient detection systems. The following section highlights solid-state pixel detectors systems in more detail and explains why they represent an interesting and valuable addition to the detector palette.

The individual detection elements of a solid-state pixel detector are patterned as a checkerboard. Each element of the sensor is connected to a matching element of the read-out electronics. The two layers are connected by, for instance, solder bumps. In this way, these hybrid detectors combine the sensor and the charge read-out in a compact way. Each sensor pixel functions as a small 'ionization chamber',^[70] in which incident particles are converted into an electron-hole pair current. The pixel size is determined by the dimensions of the read-out electronics. The dimensions of the read-out electronics scale with the complexity and size of the circuitry on the pixel level. Today, pixel pitches of 10 to 100 μm are practically accessible. Often, the read-out chip extends beyond the semiconductor sensor. This 'chip periphery' contains read-out and control circuitry, and wire-bonds for external connections. Multiple chips can be tiled together to cover larger detection areas ($>1\text{ cm}^2$). The periphery of the chips constrains full area coverage of large chip arrays without dead spaces.

Currently, two major classes of pixel detectors are being used as image sensors: charge-coupled device (CCD) sensors and complementary metal oxide semiconductor (CMOS) chips.^[70] The classic high-resolution pixel array detector is the CCD, while CMOS chips are a more recent development. The functionality, working mechanism, requirements and constraints of CCD and CMOS chips are fundamentally different. Hence, the suitability to a specific application of one or the other depends highly on the application's requirements.

4.1. CCD

Since Boyle and Smith's "Charge couple semiconductor devices" article in 1970,^[74] the CCD has not only earned its inventors the 2009 Nobel Prize (awarded "for the invention of an imaging semiconductor circuit – the CCD sensor"^[75]), but it has also developed into the most widespread wafer-scale silicon detector. CCD imagers consist of a photoactive region (typically an epitaxial layer of silicon) and a transmission region, i.e. a shift register. When a particle impinges on the image sensor, a charge proportional to the energy of the particle is generated within the sensor pixel. This charge charges a capacitor within the pixel. In a CCD chip, this charge is transported row-by-row along the column to a shift register row at the bottom of the pixel matrix. The charge is read out of this shift register row pixel-by-pixel. The last pixel in the array transfers the charge to an amplifier (typically, one to few amplifiers for the entire pixel array) and a charge-to-voltage converter. Often, an analog buffering step is included. The information collected by the CCD chip is sent off the chip as an analog signal. Sampling and digitization are performed off-chip. A CCD chip is designed and optimized to move electrical charge between capacitive bins (from pixel to pixel). Since the charge has to be transferred over thousands of pixels, the charge transfer efficiency must be close to unity so as not to lose sensitivity. Today, charge transfer is practically 100% efficient over about 10^4 pixels. The sequential readout implies relatively long readout times which scale with the area of the pixel array. CCD readout pixels can be small (10 $\mu\text{m} \times 10 \mu\text{m}$ pixels), but they achieve full area coverage.

4.2. CMOS

A CMOS chip is manufactured in the so-called CMOS technology for constructing integrated circuits. Among others, microprocessors, microcontrollers, RAM (ready-accessible memory) and many digital logic circuits are constructed in CMOS technology. Also analog circuits, like image sensors in digital cameras, can be CMOS technology based.

CMOS detection systems comprise CMOS imagers and CMOS hybrid active pixel sensors (HAPS) or detectors. The two categories are mainly distinguished by the number of transistors per pixel: CMOS imagers typically contain less than ten transistors per pixel and HAPS can contain hundreds of transistors per pixel. In hybrid pixel detectors, the sensor medium and the integrated circuit are processed on different substrates. The chip and the sensor are connected, i.e. hybridized, by fine pitch bump bonding and subsequent flip-chip attachment to a semiconductor sensor medium. Each ASIC (application-specific integrated circuit) readout pixel consists of two distinct parts: an active input region, i.e. the 'sensitive input pad', where an electron or hole current generated in the semiconductor sensor layer is received, and a logical circuitry region where the current signal is (pre-)processed.

CMOS circuits contain both p-channel and n-channel metal-oxide-semiconductor field-effect transistors (MOSFETs) on the same substrate. In a transistor, the gate (input) is capacitively coupled to the output channel that is connected between the source and the drain electrodes. In a NMOS transistor, a conductive channel is formed when the input electrode is positively biased with respect to the channel. A PMOS transistor functions complementarily. Here,

a conductive channel is formed when the gate is biased negatively with respect to the source. By connecting the source and the drain of a PMOS and a NMOS transistor, respectively, the signal that switches on one will switch off the other. The combination of a NMOS and a PMOS transistor forms a complementary MOS (CMOS) circuit. Conveniently, both the NMOS and the PMOS inverters have low static power consumption such that CMOS circuits draw no current in the high and the low state of the transistor. Since current only flows when the transistors are switching, CMOS transistors greatly reduce the power consumption in logic circuitry.

When a particle impinges on the image sensor, a charge proportional to the energy of the particle is generated within the sensor pixel of the chip. In a CMOS chip, a lot of functionality can be located on the pixel level. The density of transistors per pixel is high, hence the name 'active pixel detectors'. Typically, each pixel contains its own charge-to-voltage converter such that the charge deposited can be locally converted and digitized. Often, the pixel also comprises a (pre-)amplifier, noise corrections, discriminators or other digital signal treatment functionality. A CMOS chip outputs digital data in a predefined binary format.

4.3. The differences: CCD vs. CMOS^[70,76,77]

Figure 6 illustrates the difference between the detection of an event by a CCD or a CMOS chip. CCD imagers are typically more sensitive than CMOS imagers since their pixels are constructed for high-quality charge transport. CMOS imagers contain more per-pixel-functionality and signal treatment

efficiency. More functionality on the pixel level generally translates into more transistors and hence limits the minimum pixel size and sensitive (input pad) area.

Unlike a CMOS chip, a CCD chip cannot provide any timing information on the individual particle events. A time stamp may be assigned to a particular image frame (containing multiple events) on the basis of the CCD frame rate of typically 10 Hz – 1 kHz for standard commercial systems.

CMOS imagers can be read out faster than CCD sensors when use is made of their more parallel output structure. Concerning (read out) speed, CMOS sensors have the advantage that all camera functions can be placed on the chip. CMOS technology also enables windowing, i.e. the capability to selectively read out a portion of the image sensor. In CMOS technology, the pixel can in principle be designed to indicate the presence of a hit and to allow the selective readout of struck pixels. This increases the complexity of the pixel logic circuitry but enables higher frame rates for smaller regions of interest.

The responsivity, i.e. the amount of signal that the sensor delivers per unit of input energy, is slightly better in CMOS chips than in CCD chips since it is easier to place gain elements in a CMOS circuit. CCDs have a better image uniformity, i.e. consistency of response for different pixels under identical illumination conditions, since the CMOS in-pixel amplifiers suffer from offset variation.

CCD systems are not treated in further detail. Instead CMOS technology based systems will be focused on since the advantages of these hybrid active pixel detectors, in particular the highly parallel detection and the on-pixel functionality, offer interesting features for MS, MSI and fundamental atomic and molecular physics research.

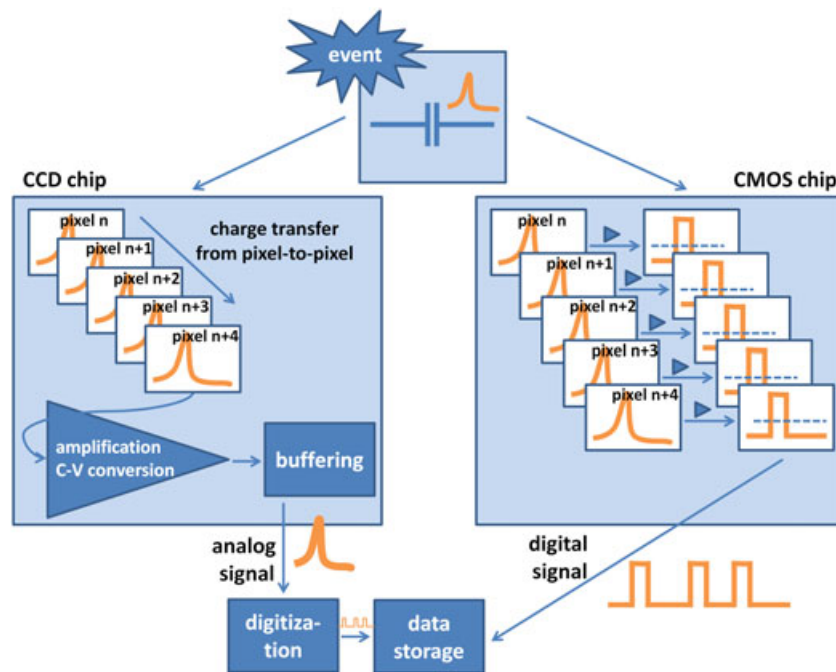


Figure 6. Event detection in a CCD chip versus a CMOS chip. For both detection systems, an electrical charge proportional to the particle energy deposited in the sensor is generated within the pixel. The deposited charge charges an in-pixel capacitor. In a CCD chip, the charge is then transferred by shift registers from pixel-to-pixel along a pixel column and an analog signal is sent off the chip. In a CMOS chip, there is significantly more functionality on the pixel level, i.e. the signal (pre-)processing takes place in the pixel and a digital signal is sent off the chip.

MSI and fundamental atomic and molecular physics research has recently used the Medipix/Timepix CMOS detector family.^[59,61,62] The following section gives a 'market overview' of a selected number of presently available and relevant CMOS imagers. These systems are contrasted to each other and to the Medipix/Timepix detector family.

4.4. CMOS imagers today: Medipix/Timepix vs. other fast pixelated detectors

4.4.1. Available CMOS systems

Many (CMOS) pixel imagers were originally developed for high-energy particle physics applications but are now readily applied to a broader range of imaging applications.^[78–80] Typically, detectors for high-energy particle physics register individual, charged quanta of radiation with a relatively high spatial and time resolution. On the contrary, many classical imaging applications, such as radiology (Medipix^[81] and MPEC^[82]) or crystallography at synchrotron light sources (XPAD,^[83–85] PILATUS^[86] and EIGER^[87]), accumulate untriggered particle events by integration or counting techniques, often with count rates in excess of 1 MHz per pixel (CT applications). The possibility to count individual particles and register extra information, as for instance the particle energy, greatly enhances the image contrast.^[88]

4.4.2. Single photon counting detectors

At the present time, a variety of different CMOS active pixel detectors are available for imaging applications. Most of these detectors are single photon counting chips, which – with some adaptations – can also more generally be used as particle-counting devices. A few examples have been selected for comparison with the Medipix2 photon-counting chip. There are other interesting CMOS active pixel detectors available. However, one or more of their specifications, such as for instance the pixel size, the pixel matrix geometry, and the operation temperature, are not suitable for (mass spectrometry) imaging applications and are therefore omitted. Therefore, we compare the Medipix2^[81,89,90] and Medipix3^[88] chips with the PILATUS II chip,^[86] the EIGER chip,^[87] the XPAD3 chip,^[83–85] and the PImMS chip^[91] (Table 3).

4.4.3. CMOS imagers with timing capabilities

Single photon counting chips do not have any timing capabilities on the pixel level. A time stamp can only be assigned to an acquired image from the camera's frame rate (typically ≤ 1 kHz, time resolution ≤ 1 ms), similar to a CCD camera. Up to now, only few CMOS active pixel detectors with timing capabilities on the pixel level have been developed. Table 4 compares the Timepix^[92] chip with the NA62 collaboration's timing chip.^[93–97]

Table 4 shows that the Timepix is currently the most obvious and practical choice for many imaging applications in MS, MSI, atomic and molecular physics research and beyond. The current Timepix chip already delivers a reasonable time resolution and the next generation of chips will improve this significantly (see section 5.1.5). In addition, the pixel size, the large pixel matrix, the tileability to larger areas, and the very high fill factor make the Timepix attractive. The NA62 chip, on the other hand, delivers outstanding time resolution and

measurement range for TOF experiments. However, the large pixel size, the small pixel matrix and the cooling requirements make this chip less attractive for imaging applications.

There are a few other ultra-high time resolution CMOS-based developments. Jansson and co-workers have designed an ultra-high time resolution CMOS circuit, which has a time resolution of 12.2 ps and measurement range of 204 μ s.^[98] Another interesting development is the CMOS-based single photon avalanche diodes (SPADs) of Charbon and co-workers.^[99–101] These detection devices achieve a time resolution down to 50 ps. However, the maximum measurement time is tens to hundreds of nanoseconds, which is insufficiently long for TOF MS but the devices are used for on-chip fluorescence detection and fluorescence lifetime imaging microscopy.^[102] In addition, the fill-factor of the SPADs is only 2% (up to 14% using microlenses) such that a full event coverage cannot be achieved with the detection system and high spatial resolution imaging is inaccessible.

5. THE MEDIPIX/TIMEPIX DETECTOR FAMILY

5.1. Chips of the Medipix/Timepix detector family

The Medipix detector family is being developed within the Medipix collaboration hosted by CERN.^[103] Currently, the Medipix collaboration consists of about 20 collaborating institutes from all over the globe that work together on the development of the Medipix chips, readout interfaces and software packages for various applications ranging from high-energy particle physics to medical X-ray imaging.^[90] The chips of the Medipix detector family in combination with a detection medium – often a semiconductor like silicon bump-bonded on top – belong to a new class of hybrid pixel detectors. There are two distinct types of chips within the Medipix detector family: the Medipix single photon counting chips and the Timepix chips, which in addition to the single photon counting capabilities can also be set to measure the time-of-arrival of an event with respect to an external reference signal or to determine the amount of charge deposited per pixel. Thus far, three generations of Medipix chips and one generation of the Timepix chip have been developed. Developments of new (variants of the) chips are ongoing. In MSI and atomic and molecular physics research, so far chips of the Medipix2^[81,89,92] generation, i.e. the Medipix2 and the Timepix chips, have been used. Table 5 contains a comparison of all the chips of the Medipix/Timepix detector family.

5.1.1. Medipix1

The Medipix chip (or PCC, photon-counting chip)^[104] was originally designed for counting X-ray photons, without noise or dark current, at high particle fluxes (several gigaphotons per square-cm per second). The Medipix1 chip consists of 64×64 pixels with a pixel size of $170 \mu\text{m} \times 170 \mu\text{m}$. Each of the identical pixels has a preamplifier, a discriminator and a 15-bit counter. The chip was bump-bonded to silicon (Si) and gallium-arsenide sensors (GaAs) for direct photon conversion and hence minimum image blurring.

Table 3. Comparison between selected state-of-the-art single photon counting chips

Feature	Medipix2	Medipix3	PILATUS II	EIGER	XPAD3	PImMS
Technology	0.25 μm CMOS	0.13 μm CMOS	0.25 μm UMC	0.25 μm UMC	0.25 μm CMOS	CMOS
Single photon counting	yes	yes ^{\$}	yes	yes	yes	yes
Pixel size [$\mu\text{m} \times \mu\text{m}$]	55 \times 55	55 \times 55	172 \times 172	75 \times 75	130 \times 130	70 \times 70
Pixel array	256 \times 256	256 \times 256	60 \times 97	256 \times 256	80 \times 120	512 \times 512
Pixels/chip	65536	65536	5820	65536	9600	262144
Chip tiling	2 \times 2n	2 \times 2n	2 \times 8	2 \times 8 (=module), $\leq 4 \times 8$ modules	7 \times n	N/A
Typical sensor materials	Si, GaAs, CdZnTe, CdTe, Ge	Si	Si	Si	Si, CdTe, GaAs, Shottky sensors	N/A
Sensor sensitive thickness	150–300 μm (Si), 0.5 mm (GaAs), 1–2 mm (Cd(Zn)Te)	150–300 μm (Si), 0.5 mm (GaAs), 1–2 mm (Cd(Zn)Te)	320 μm	300–500 μm	500 μm	N/A
ENC ^{††} / electrons per pixel	100	60–180 [#]	114	180	100–160	N/A
Power dissipation per pixel	15 μW	9–15 μW [†]	10 μW	12 μW	40 μW	30 μW
Maximum number of frames/second ^{††}	500	1000	200–416	24 k / 12 k / 8 k (4/8/12 bit mode)	200–300	20
Dead/read-out time	1 ms	0 ⁺⁺	2.4 ms	3 μs ^{##}	N/A ^{\$\$}	N/A
Counter depth [bits]	13	Configurable: 1, 4, 12, 24 [†]	20	Configurable: 4, 8, 12, 32 [±]	12 + overflow bit	N/A
Charge sharing between multiple pixels	yes	limited ^{**}	'not an issue'	yes	yes	N/A
Online correction mechanisms	- bad pixel map	- charge summing mode - bad pixel map	- energy & gain setting dependent rate correction - flat field correction - bad pixel map	N/A	no	N/A

^{\$}There are different single photon counting modes: (1) pitch versus spectroscopic mode, (2) single pixel versus charge summing mode, (3) low versus high gain mode.

^{††}The ENC for chips with/without sensor is different (see section 5.1.2). The numbers stated in the table give an indication of the ENC.

[#]The ENC depends on the operation mode of the chip.

[†]15 μW /pixel (charge summing mode), 9 μW /pixel (single pixel mode).

⁺⁺This number corresponds to the frame rate when the entire chip is read out.

^{##}Depending on the operation mode. In continuous readout mode, there is no dead time.

^{\$\$\$}The frames are comparatively short because of the implemented double buffering. The next frame is acquired, while the previous frame is read out.

^{\$\$\$}Measurements beyond the 12-bit register depth are enabled by the 13th bit, i.e. the overflow bit. The overflow bit registers how many times the 10-bit register has been filled. Readout of the overflow bit and the 10-bit register takes place after the acquisition.

[†]The bit depth is configurable to 1, 4, 12 bits in both the sequential and the continuous acquisition mode, and to 24 bits in sequential mode only.

[±]A counter depth of 32 bits is a 'virtual' counter depth. This is accessible if several images are summed on the readout control board. This is implemented to reduce the data throughput for long exposure times.

^{**}Here, the charge in every cluster of 4 pixels can be summed and assigned to the pixel with the largest charge asynchronously on an event-by-event basis.

N/A During the writing of this article, no information on the particular parameter was available (yet) since these systems are still under development.

Table 4. Comparison between two selected state-of-the-art HAPS, the Timepix and the NA62 chips

Feature	Timepix	NA62 chip
Technology	0.25 μm CMOS	0.13 μm CMOS
Counting modes	<ol style="list-style-type: none"> 1. event counting 2. time-of-flight (TOF) 3. time-over-threshold (TOT) 	<ol style="list-style-type: none"> 1. time-over-threshold (TOT) 2. event counting: by counting TOT events 3. time-of-flight (TOF)
Pixel size [$\mu\text{m} \times \mu\text{m}$]	55 \times 55	300 \times 300
Pixel array	256 \times 256	45 \times 40
Pixels/ chip	65536	1800
Chip tiling	2 \times 2n	2 \times 5
[n = 0,1,2,...]		
Typical sensor materials	Si	Si
Sensor sensitive thickness	300 μm	200 μm
ENC ^{††} /electrons	100–113 electrons	130–185 electrons
Power dissipation per pixel	15 μW	1.8 mW
Maximum number of frames/s [^]	30–50	~73 khits/s per pixel
Dead time/readout time	300 μs /10 ms [‡]	Per 5 pixels: 10 ns
Counter depth [bits]	13	Infinite*
ASIC binning time, i.e. time resolution	10 ns	100 ps
Charge sharing between multiple pixels	Yes	Yes
Online correction mechanisms	No	No
Field of view selection	No	Yes, by masking a pixel it is taken off the data path and the data bandwidth is increased

††The ENC for chips with/without sensor is different (see section 5.1.2). The numbers stated in the table give an indication of the ENC.
[‡]For a 100 MHz readout clock, the chip can be read out serially (all 32 CMOS lines in series) in 10 ms. When reading out the CMOS lines in parallel, the readout takes 300 μs .
*The basic time bin is 100 ps. Hence, the dynamic range extends to 6.4 μs . However, the chip is certainly read out within these 6.4 μs . The readout electronics board keeps track of how many times 6.4 μs are 'filled' by events. In this mode of operation, there is no dead time and the counter depth is infinite.

Table 5. Comparison of the Medipix1, Medipix2, Medipix3 and Timepix chips

Feature	Medipix1	Medipix2	Medipix3	Timepix
Technology	1 μm SACMOS [‡]	0.25 μm CMOS	0.13 μm CMOS	0.25 μm CMOS
Acquisition modes	Single photon counting	Single photon counting	Single photon counting Modes: 1. fine pitch/spectroscopic 2. single pixel/charge summing 3. low/high gain	1. Single photon counting 2. Time-of-flight 3. Time-over-threshold
Pixel size [$\mu\text{m} \times \mu\text{m}$]	170 \times 170	55 \times 55	55 \times 55	55 \times 55
Number of pixels per chip	64 \times 64 = 4096	256 \times 256 = 65536	256 \times 256 = 65536	256 \times 256 = 65536
Sensitive to charge	positive	positive or negative	positive or negative	positive or negative
ENC ^{††} /electrons	170	100	60–180	100–113
Power dissipated	N/A	15 μW / pixel	15 μW /pixel (charge summing mode), 9 μW / pixel (single pixel mode)	15 μW / pixel
Dead time	384 μs @ 10 MHz	1 ms	None [#]	300 μs /10 ms [§]
Dynamic range	15 bit	13 bit	Programmable to 1-, 4-, 12-bits (in sequential & continuous acquisition mode); 24-bits only in sequential mode	13 bit
Energy range*	>4–5 keV [†]	>4–5 keV [†]	>4–5 keV [†]	>4–5 keV [†]

[‡]SACMOS = self-aligned contact CMOS

^{††}The ENC for chips with/without sensor is different (see section on 5.1.2). The numbers stated in the table give an indication of the ENC.

*The particle energy range that can be detected depends on the sensor material and thickness. This row indicates a few typical values.

[#]The chip can be configured to work in the continuous readout mode in which there is no dead time due to readout.

[§]For a 100 MHz readout clock, the chip can be read out serially (all 32 CMOS lines in series) in 10 ms. When reading out the CMOS lines in parallel, the readout takes 300 μs .

[†]This energy corresponds to the deposition of about 1500 electrons in a silicon sensor.

N/A During the writing of this article, no information on the particular parameter was available (yet) since these systems are still under development.

5.1.2. Medipix2

The Medipix2^[81,89,92] detector is the successor of the earlier Medipix1 chip. The dimensions of a single Medipix chip are $1.4\text{ cm} \times 1.6\text{ cm}$ and the pixel matrix contains 256×256 pixels of $55\text{ }\mu\text{m} \times 55\text{ }\mu\text{m}$ each. The chips are three-side buttable so that chip arrays of $2 \times 2n$ chips ($n=1,2, \dots$) can be tiled without dead space between the chips.

The Medipix2 chips are typically combined with a semiconductor detection medium bump-bonded on top. The semiconductor materials are silicon, gallium-arsenide, cadmium telluride, cadmium-zinc-telluride or germanium, depending on the application of the detection system (see section 5.2). Typically, a $300\text{ }\mu\text{m}$ silicon sensor (lightly n-doped high-resistivity silicon with a p-type implant in every pixel) is bump-bonded on top of a Medipix chip. On the entrance side, the sensor layer is coated with an aluminum layer of about 150 nm . Through this Ohmic contact, the sensor material is biased by applying a voltage of about 100 V across the sensor. An electron or a hole current can be collected by the pixels. In silicon, every 3.6 eV of deposited energy creates one electron-hole pair. Hence, the amount of charges generated in the sensor material is directly proportional to the energy deposited by the impinging particle. With such a sensor layer photons and electrons can efficiently be detected, provided that the photon or electron kinetic energy exceeds the detection threshold of about $4\text{--}5\text{ keV}$.

When used for X-ray and electron detection, the detection medium converts incident particles into electron-hole pairs, which induce a current in the charge-sensitive amplifier of the CMOS (complementary metal oxide semiconductor) readout chip. Ions will usually not be accelerated to sufficient energies to penetrate into the sensor layer. However, ions can be detected indirectly by placement of an MCP in front of the detector.^[33,61] The Medipix detector then registers the electron shower produced by each ion impact on the MCP. The particle-counting properties consist of the ability to count events that generate a number of electron-hole pairs within a user-defined threshold/energy window.

Each individual pixel comprises an analog and a digital part. The analog input stage consists of a preamplifier and two identical pulse height discriminators. These discriminators generate a digital pulse if the output of the preamplifier falls within a predefined energy window. These digital pulses increment a 13-bit pseudo-random counter. A pseudo-random counter is a linear feedback shift register. In this type of shift register, each successive register value is generated by a feedback loop from the previous register value. Since all successive register values are predictable and known, these registers can be used as counters. Every register reading encodes a counter value. The shift register values can be converted into ordinary, decimal counter values via a look-up table. Pseudo-random counters are set up such that the combination of binary values in the register is always composed of roughly the same number of ones and zeros. This prevents rapid voltage changes when the counter value is incremented, which is desirable for densely packed electronic circuits like the Timepix chip. Other advantages are that pseudo-random counters are fast counters and that they can be implemented in hardware.

The threshold energies that are chosen for the discriminator levels lie just above the noise levels of the pixels. Therefore, electronics noise-free measurements are possible. Three additional adjustment bits can be used to equalize the pixel-to-pixel response over the full pixel array.

Equivalent noise charge

For both Medipix2 and Timepix chips, the minimum detectable charge per pixel is given by the pixel's noise, i.e. by the 'equivalent noise charge' (ENC).^[105] By convention, the minimum charge required to trigger an above-pixel-noise signal is set to 6 times the ENC. The ENC per pixel was determined to be 100 electrons for a bare chip and 113 electrons for a chip bump-bonded to a $300\text{ }\mu\text{m}$ silicon sensor layer. Thus, the minimum detectable charge is approximately 600 electrons for a bare chip pixel and approximately 678 electrons for a chip pixel with a $300\text{ }\mu\text{m}$ silicon sensor layer. The overall chip minimum detectable charge is estimated by adding the pixel-to-pixel mismatch. Typically, a Timepix chip shows a pixel-to-pixel threshold mismatch of about 35 electrons if properly threshold equalized (i.e. if the response of the pixels is homogenized) and a pixel-to-pixel threshold mismatch of about 250 electrons if it is not equalized. Therefore, a bare Timepix chip has a minimum detectable charge of $6 \cdot \sqrt{(100^2 + 35^2)} = 635$ electrons for an equalized chip and 1616 electrons for a non-equalized chip, respectively. A Timepix chip with a $300\text{ }\mu\text{m}$ silicon sensor layer has a minimum detectable charge of 710 electrons for an equalized chip and 1646 electrons for a non-equalized chip. Importantly, these numbers of electrons can easily be achieved in the electron showers that results from the impact of an ion on a chevron MCP detector (even at sub-saturation MCP gains).

5.1.3. Timepix

The Timepix chip^[92] is derived from the Medipix2 chip design. Figure 7 displays a microscope image of a bare Timepix chip. The dimensions and geometry of the chip are identical to those of its predecessor but the functionality on the pixel level is different. Each pixel can be individually selected to operate in one of three modes:

- (1) **The event-counting mode:** Each pixel counts the number of events. This mode is particularly interesting for integrated image detection.
- (2) **The time-of-flight (TOF) mode:** The occurrence time of an event is measured with respect to an external trigger/shutter signal (Fig. 8). The chip returns the localization of the event via the pixel address (x - and y -coordinate) and



Figure 7. Microscope image of part of a bare Timepix chip.

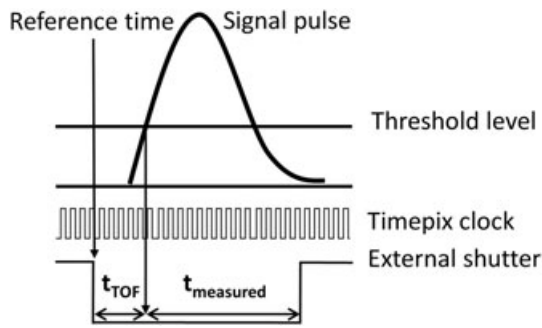


Figure 8. Schematic representation of the working mechanism of the TOF mode. The TOF of an event is measured with respect to an external shutter. When an above-threshold signal is induced in the pixel, the pixel counter counts clock cycles until the end of the external shutter interval. The TOF can then be determined from: $\text{TOF} = t_{\text{shutter}} - t_{\text{measured}}$.

the corresponding TOF. In MSI and VMI, this mode can both be used for selected image detection and spectral image detection.

- (3) **The time-over-threshold (TOT) mode:** The time is measured during which the charge resulting from the event exceeds the detection threshold level (Fig. 9). The chip returns the localization of the event via the pixel address (x- and y-coordinate) and the corresponding TOT, i.e. a measure for the charge deposited on the pixel. Ultra-high resolution images can be generated with this mode.^[33] If an event covers multiple pixel elements, the TOT information of the event distribution reflects the charge distribution throughout the event. Using this intensity information, the centroid of the event distribution can be computed using a centroiding algorithm.

The maximum measurement time in TOF and TOT mode is determined by the pixel counter depth times the measurement clock speed. The Timepix pixel counter is a 13-bit pseudo-random counter. The maximum counter value of the Timepix chip is 11810, i.e. 11810 is the pixel overflow value. This overflow value, 11810, represents the number of possible pseudo-random counter values (values with roughly equal amounts of ones and zeros) for the Timepix chip. Therefore, at the maximum clock speed of 100 MHz (i.e. 10 ns clock cycles), a maximum measurement interval of $11810 \cdot 10\text{ns} = 118.1 \mu\text{s}$ is available.

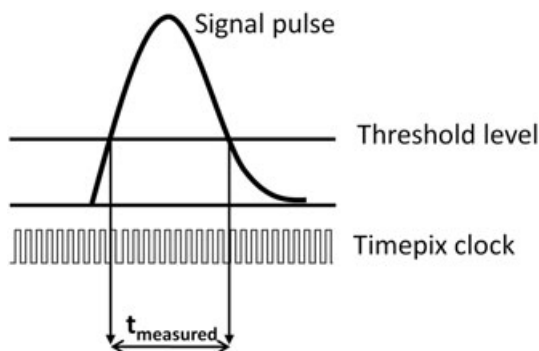


Figure 9. Schematic representation of the working mechanism of the TOT mode. The TOT of an event is measured by counting the number of clock cycles during which the pixel is over the threshold.

Each individual pixel in the chip can be programmed to operate in one of the three modes. Hence, it is possible to use the chip in 'checkerboard' mode (or any other desired pattern) where half the pixels are programmed to operate in the TOF mode and the other half in the TOT mode. If events cover multiple pixels, such an arrangement enables the measurement of the TOF of the event and the high-resolution position determination via a centroid calculation (if the overlap between multiple events on the detector is limited).

In MSI and VMI so far, chips without a sensor layer, so-called bare chips, have been used to improve the response to electron showers through reduced in-sensor electron diffusion, i.e. by reducing the charge sharing between neighboring pixels.^[106-109] In other applications, a metal grid on insulating pillars can be suspended above the chip,^[110] a so-called micromegas.^[111] The space between the ASIC and the grid is filled with an interaction gas, in which charge amplification occurs due to an electric field bias voltage. These systems are typically used as time-projection chambers and will not be treated in further detail here.

5.1.4. Medipix3

The Medipix3 chip^[88] is a single photon counting chip that has the same geometry as the Medipix2 chip. However, the inter-pixel architecture is fundamentally changed in order to reduce the effect of charge sharing between multiple detector pixels. Charge summing between groups of 2×2 pixels has been introduced. Within such a cluster of pixels, the information obtained by individual pixels is combined to reconstruct the total charge which is then assigned to the pixel with the largest charge. In this way, the $55 \mu\text{m}$ spatial resolution is maintained, while the spectral distortion due to charge diffusion in the sensor layer is reduced. The Medipix3 chip can be operated in several configurations:

Fine pitch mode versus spectroscopic mode: In the fine pitch mode, every pixel of the chip is connected to a sensor element of the same pitch ($55 \mu\text{m}$) as typically done for the Medipix2 chip. In the spectroscopic mode, only one pixel per cluster of 2×2 pixels is connected to a sensor pixel of $110 \mu\text{m}$ pitch. As every $55 \mu\text{m}$ pixel has two discriminators and two counters, the resulting $110 \mu\text{m}$ pixel can use up to eight thresholds and counters.

Single pixel or charge summing mode: As in the current Medipix2 chip, each pixel works as an individual photon-counting element independent of its neighboring pixels in the single pixel mode. Charge summing between groups of 2×2 pixels has been introduced. Within such a cluster of pixels, the information obtained by individual pixels is combined to reconstruct the total charge which is then assigned to the pixel with the largest charge. In this way, the $55 \mu\text{m}$ spatial resolution is maintained, while the spectral distortion due to charge sharing in the sensor layer is eliminated. Charge summing can be used both in the fine pitch and in the spectroscopic mode.

High gain mode versus low gain mode: The pixels can be run at high or at low gain.

Data acquisition and read-out sequentially or continuously: In the sequential acquisition mode, two threshold levels and both of the pixel's 12-bit counters can be used, i.e. a 24-bit counter depth. Readout occurs after each acquisition and results in a dead time. In the continuous acquisition mode,

only one threshold level and one 12-bit counter are available for the measurement, while the other one is readout. There is no dead time due to readout in the continuous acquisition mode.

The Medipix3 is particularly interesting for integrated image detection. In the spectroscopic mode, the eight thresholds and counters will enable color X-ray imaging, for instance. In addition, the charge summing mode can provide higher resolution images by counteracting the 'charge sharing' effect between neighboring pixels.

5.1.5. Future Medipix/Timepix chips

At this point, the collaboration has decided to add two new ASICs to the Medipix detector family, the Timepix3 and the SmallPix chips. The design specifications for both chips have not been finalized at the point of writing this article and may be subject to changes. Planned design features that are particularly interesting to the field of mass spectrometry (imaging) and fundamental atomic and molecular physics research are highlighted.

The Timepix3 chip will probably have the same dimensions as the Medipix2/Timepix chip. Major differences between the Timepix and the Timepix3 chips are that the Timepix3 chip will acquire both the time-of-arrival and the time-over-threshold in two separate registers in each pixel. In addition, the Timepix3 will have a so-called 'data-push' read-out, i.e. pixel readout occurs on an event-by-event basis rather than by reading out the entire pixel matrix at the end of the measurement interval. The pixels that are being read out are dead and cannot accommodate any new events during readout. However, the rest of the pixel matrix can still acquire data. Therefore, the data-push readout removes an overall dead time due to reading out the entire pixel matrix at the end of a measurement interval. The time measurements of the Timepix3 will have a higher timing resolution than the current Timepix chip.

As the name 'Smallpix3' suggests this chip will deviate from the 55 μm pixel pitch of the Medipix2/Timepix chips. An obvious advantage of a smaller pixel pitch is an increase in spatial resolution. Through the implementation of super-pixels a larger available bit depth (and hence longer measurement time, for instance, in TOF mode) could be obtained.

5.2. Chips with/without a sensor layer

5.2.1. Sensors^[112]

The semiconductor layer on top of the ASIC is typically referred to as a 'sensor' in the field of ASICs. The chips of the Medipix/Timepix detector family are typically combined with a semiconductor [note that materials are classified as semiconductors if their electrical resistivity is about 10^3 to $10^9 \Omega \text{ cm}$ and their band gap is a few eV] sensor. The pixels of the semiconductor sensor material assume the same pitch as the chip's pixels. Each sensor pixel is attached to an ASIC pixel by a solder bump ('bump-bonding'). The choice of sensor material largely depends on the intended application of the chips. Silicon is commonly used as a 'multi-purpose' sensor for particle detection, for instance, in tracking applications in high-energy particle physics. However, its stopping power for photons with energies higher than of 20 keV is low. Since the photon energies in medical radiography can be significantly higher, alternative, high-Z sensor materials are required. Gallium-arsenide, cadmium telluride, and

cadmium-zinc-telluride are possible sensor alternatives. These room-temperature semiconductor materials are typically used for high-energy X-ray and γ -ray detection. However, the production of large areas of homogenous, defect-free sensor materials is challenging. Germanium, although requiring to be cooled to liquid nitrogen temperatures, is used for X-ray experiments at synchrotron light sources.^[113,114]

5.2.2. Sensor layer or MCP?

When used for X-ray and electron detection, the detection medium converts incident particles into electron-hole pairs, which are collected in the charge-sensitive amplifier of the CMOS readout chip. The charge created in the sensor layer typically spreads out over multiple pixels. This charge sharing effect blurs the image. Ions typically do not have sufficient energy to penetrate into the sensor layer. Ions can be detected indirectly by placing a MCP in front of the detector.^[33,61] The (bare) chip then registers the electron shower produced by each ion impact on the MCP. The introduction of an MCP decreases the detection efficiency due to the 70 to 80% fill factor of the MCP.

5.3. Tiling to larger areas

For large-area imaging applications, seamless detectors can be desirable. This still poses a challenge. A single chip has an area of about 2 cm^2 . However, many (imaging) applications require larger detector areas. Currently, the three-sided buttable chips can be arranged in rectangular $2 \times 2n$ ($n=1, 2, 3, \dots$), full-coverage arrays of chips. Larger detector areas can be achieved by tiling multiple 2×2 units of detector together as, for instance, suggested by the ReLAXD project.^[115] A drawback of tiling larger areas from four-chip units is the inactive space between detector modules. This dead space is due to the periphery of the chips and the wire-bonds that are located on one side of the ASIC (Fig. 10).

A step towards the reduction of dead space between chips is through the use of silicon vias (TSVs),^[116] i.e. vertical electrical connections through the silicon chip, which replace the wire-bonds. The TSVs enable a more compact chip periphery and, therefore, reduce the inactive space in large-area, multi-pixel arrays. Unlike wire-bonds, the TSVs do not extend above the chip surface. Therefore, larger semiconductor sensor layers ($> 2 \times 2$ chip array) can be connected to the chip array. The sensor size can, however, still limit the detector area depending on the semiconductor sensor material. The production of large-area semiconductor sensors is still difficult. Si sensors are routinely produced up to 12 inches in diameter (circular), GaAs up to 6 inches, and CdTe up to 3 inches.

5.4. Readout hardware and software for the Medipix/Timepix detector family

5.4.1. Control and acquisition software

Most users within the collaboration control and interact with the chips using the dedicated acquisition software 'Pixelman'^[117,118] developed and maintained by the Pospisil group. Pixelman allows the user to set up measurements, equalize the pixels and test the chips (digital and analog tests, test pulses, etc.). In addition, the user can extend the

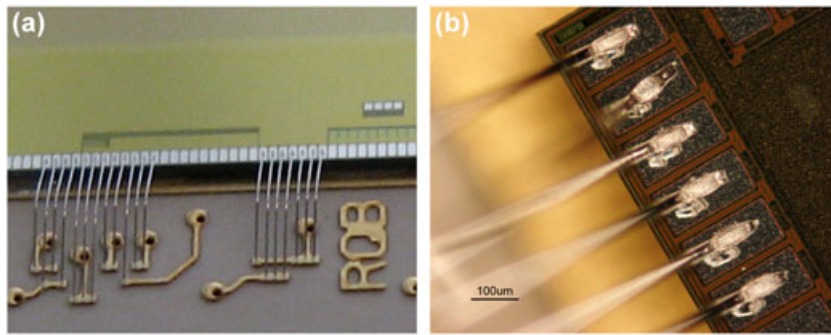


Figure 10. (a) Photograph of part of a Timepix chip mounted on a vacuum-compatible chip carrier. The chip periphery, wire-bond pads and wire-bonds are displayed. (b) Microscope image of part of a Timepix chip. Part of the chip periphery, the on-chip wire bond pads and wire-bonds are shown.

functionality of Pixelman via plug-ins. There are also a few alternative control and readout software packages, which have specifically been developed for a particular readout interface.

Among other file formats, the data from the chips can be saved in ASCII (American Standard Code for Information Interchange) format. Typically, the data is saved sparsely, i.e. only pixels that have registered an event are listed in the output data file. The data file is organized in three columns, the x- and y-coordinate of the pixel and the number of events (Medipix mode), time-over-threshold or the time-of-flight. The data-processing software depends largely on the specific application in which the ASICs are used.

5.4.2. Hardware

USB

A number of universal serial bus (USB) readout interfaces have been designed by the Pospisil group: the USB 1.0 readout,^[119] the USB Lite,^[120] the USB 2.0 Rapid Universal Interface (RUIIN), and the Fast Interface for Timepix Detectors (FITPIX)^[121] readouts. Conveniently, these readout boards directly click into the ASIC carrier and the necessary voltages are internally derived from the voltage provided by the USB connection such that no external power supplies are needed. These compact readout interfaces are very well suited for portable measurement setups.

MUROS2

The MUROS2 readout^[122] represents an interface between the Medipix2 chip and a general-purpose commercial PCI-based acquisition card (National Instruments Corporation, Austin,

TX, USA). The on-board field-programmable gate array (FPGA) transmits data between the chip(s) and the measurement PC. In addition, the board comprises a number of registers to control the chip operation. Per chip, the CMOS data lines are read out in series. The MUROS2 is designed to read out chip carriers with a maximum of eight chips. Individual chips are read out in series (daisy chain).

ReLAXD readout

The ReLAXD readout^[115,123] is a gigabit per second (1 Gbit/s) readout system developed within the framework of the ReLAXD project (high Resolution Large Area X-ray Detector) (Fig. 11). The ReLAXD module reads out the four chips of a 2×2 chip array in parallel (CMOS lines in series) and achieves frame rates of up to 120 Hz. The user interacts with the chip via the dedicated acquisition software and graphical user interface Pixelman or the so-called ReLAXD DAQ, dedicated readout and control software for the ReLAXD module.

The ReLAXD board needs a supply voltage of about 12 V and provides the Timepix ASICs with the required supply voltages. An on-board FPGA (Lattice LFSC15, Lattice Semiconductor Corporation, Hillsboro, OR, USA) controls the signals to and from the chips. The board communicates with the measurement PC via standard 1 Gbit/s Ethernet such that the hardware requirements are a 1 Gbit/s Ethernet cable (1 Gbit/s, CAT. 5, STP) and a 1 Gbit/s Ethernet card (Intel PRO/1000 PT Server Adapter, Intel Corporation, Santa Clara, CCA, USA) in a measurement PC. The ReLAXD readout board and the chip carrier are clicked together in a T-shape configuration.

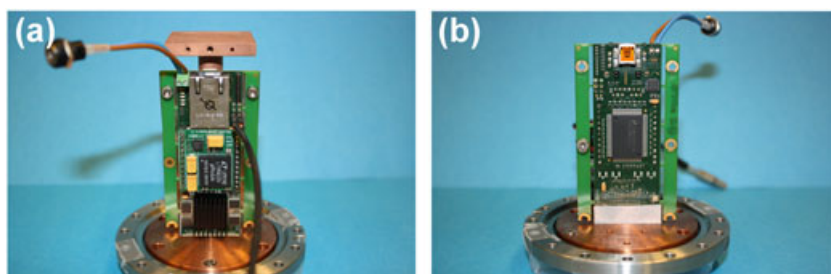


Figure 11. ReLAXD read-out board: (a) top and (b) bottom side.

The measurement clock of the Timepix is derived from a 25 MHz local oscillator and can be set between 5 MHz and 100 MHz in steps of 5 MHz. This results in a minimum time resolution of 200 ns and a maximum time resolution of 10 ns. An external trigger (start and stop) can be applied to the chips via the ReLAXD board's external trigger input. Using the Pixelman readout software, the chips can be tested, and the adjustment and measurement parameters can be set. A maximum number of 10 to 30 readout frames per second (frames/s) can be reliably achieved with Pixelman (for acquisition time \ll read-out time). Using the ReLAXDAQ software, one can read out about 120 frames/s. In Pixelman, the frame rate is limited by the online 'de-randomization' of the pixel counter values, while the ReLAXDAQ reads out the frames untreated and the de-randomization is carried out offline. So far, the ReLAXDAQ is a pure readout program with limited features to configure the chips. It is possible to prepare the chips for a measurement in Pixelman and then use the faster ReLAXDAQ to acquire the data. Data de-randomization has to be carried out offline.

Berkeley Quad Timepix Parallel Readout

The Berkeley Quad Timepix Parallel Readout^[124] represents a highly parallel readout system dedicated to measurement setups using 2×2 Timepix ASICs. The readout system reads out all four chips and all 32 CMOS signal lines from the parallel ASIC output at the same time. A frame rate of about 1 kHz can be achieved.

The Berkeley readout consists of three subsystems. The first element of this system is the ASIC carrier on which the four Timepix chips are mounted. The CMOS signal of two chips is read out from the ASIC carrier by the second subsystem, i.e. two interface boards. On these two interface boards, a field-programmable gate array (FPGA) converts the digital data from the ASIC into LVDS (low-voltage differential signaling) logic levels. In this format, the data flows to the third part of the system, in particular to the ROACH (Reconfigurable Open Architecture Computing Hardware) board. The ROACH board is a stand-alone FPGA-based processing board on which events are extracted from the data stream and passed on to the measurement PC via a 10 Gbit/s Ethernet connection. It should be noted that saving the entire pixel matrix poses a challenge at such high frame rates, which limits the applicability to high count rate experiments.

More read-out systems

Within the collaboration, several read-out interfaces have been developed to target specific applications. Among others, there is the 'Parallel Readout Image Acquisition for Medipix' (PRIAM)^[125] system for reading out the Medipix2 chip at kilohertz frame rates. The 'Dear-Mama Acquisition System' (DEMAS)^[126] reads out the Medipix2 chip at 500 Hz and is capable of both data transfer modes, i.e. chip readout via the serial LVDS lines and chip readout via the 32-bit CMOS parallel bus. Another gigabit Ethernet readout system was developed for use in the 'Medipix All Resolution System computed tomography' (MARS-CT) scanner. A 'Speedy Pixel Detector Readout' (SPIDR) for 1 kHz operation is under development.

6. ALTERNATIVE IMAGING DETECTORS

In the last two years, a number of alternative (ion) imaging detectors have been brought into operation, a few of which are highlighted below.

IonCCD

The ionCCD (OI Analytical, Pelham, AL, USA)^[127] is a modified CCD array detector for direct charged particle imaging. In particular, the semiconductor part of the CCD (in which the electron-hole pair current is generated upon photon impact) is replaced by a conductive layer of TiN. The conductor collects charge from the impinging ions by charge neutralization. The ionCCD consists of 2126 pixels. Each pixel has dimensions of $21 \times 1.5 \mu\text{m}^2$. There is a $3 \mu\text{m}$ gap between individual pixels. The fill factor of the ionCCD is 87.5%. Hadjar and co-workers have successfully tested the ionCCD for electrons and (biomolecular) ions.^[128,129] They report that the detection efficiency of the ionCCD does not depend on the ion energy, flux and angle of incidence. However, the detection efficiency is directly dependent on the charge state of the incident ion. The quantum efficiency of the chip is about 25–33%. These authors have established the ionCCD as a robust, high potential electron and ion analyzer, which could also be employed as a pixelated readout anode for MCP-based detection systems.

Single photon avalanche photodiode (SPAD)

Similar to the work of Charbon and co-workers,^[99–101] Wilman and co-workers have implemented a commercial photon-counting silicon detector (Hamamatsu multi-pixel photon-counting (MPPC) sensor) in combination with a scintillator for TOF MS.^[130] The ion impinges on the scintillator and causes photon emission. The photons are registered by the silicon sensor of the SPAD. The active area of this sensor is 1 mm^2 and the pixel pitch is $25 \mu\text{m}$. While the time resolution of the MPPC is of the order of 200–300 ps, the achievable time resolution (and hence mass resolution) is limited by the $\sim 40 \text{ ns}$ decay time of the scintillator. The authors suggest that an improved version of the scintillator-SPAD detector system could provide a valuable alternative to MCP-based detection systems. Improvements should include a shorter decay time scintillator for more competitive time/mass resolution measurements and larger area detectors (possibly in the form of SPAD arrays).

7. CONCLUSIONS

Detector technology for ions, electrons and photons has greatly advanced over the past decades. Depending on the specific application, several fundamentally different detection mechanisms for ions, electrons and photons have successfully been put into operation. Many novel detector concepts for integrated image detection, selected image detection or spectral image detection have been proposed and are on their way to routine operation. The choice of a specific detection mode and corresponding detector system is largely application-dependent. However, most modern experiments demand high-performance, robust technology, which delivers precise particle detection. The developments of the past

years – hybrid active pixel detectors, single photon avalanche photodiodes and the ionCCD among others – are highly exciting pieces of technology. In particular, the Medipix/Timepix active pixel detector family has high potential for high-resolution, time-resolved imaging applications in MS and MSI, fundamental atomic and molecular physics research, and beyond. These detection systems provide unique analytical capabilities and operational attributes, which conveniently complement the existing particle detection toolbox.

Acknowledgements

Part of this research is supported by the Dutch Technology Foundation STW, which is the applied science division of NWO, and the Technology Programme of the Ministry of Economic Affairs, Project OTP 11956. This work is part of the research programme of the Foundation for Fundamental Research on Matter (FOM), which is part of The Netherlands Organisation for Scientific Research (NWO). The authors acknowledge Marten Bosma for scientific discussions and Dirk-Jan Spaanderman for designing Fig. 2.

REFERENCES

- [1] *Webster's New World Dictionary & Thesaurus*, Simon & Schuster Inc. **1996**.
- [2] J. H. Barnes, G. M. Hieftje. Recent advances in detector-array technology for mass spectrometry. *Int. J. Mass Spectrom.* **2004**, *238*, 33.
- [3] A. J. H. Boerboom. Array detection of mass-specra, a comparison with conventional detection methods. *Org. Mass Spectrom.* **1991**, *26*, 929.
- [4] J. L. Wiza. Microchannel plate detectors. *Nucl. Instrum. Methods A* **1979**, *162*, 587.
- [5] A. S. Tremsin, O. H. W. Siegmund. Spatial distribution of electron cloud footprints from microchannel plates: Measurements and modeling. *Rev. Sci. Instrum.* **1999**, *70*, 3282.
- [6] A. Vredenburg, W. G. Roeterdink, M. H. M. Janssen. A photoelectron-photoion coincidence imaging apparatus for femtosecond time-resolved molecular dynamics with electron time-of-flight resolution of $\sigma = 18$ ps and energy resolution $\Delta E/E = 3.5\%$. *Rev. Sci. Instrum.* **2008**, *79*, 063108.
- [7] R. J. Wenzel, S. Kern, R. Zenobi. Proc. 54th ASMS Conf. Mass Spectrometry and Allied Topics, Seattle, USA, **2006**.
- [8] A. van Remoortere, R. J. M. van Zeijl, N. van den Oever, J. Franck, R. Longuespee, M. Wisztorski, M. Salzet, A. M. Deelder, I. Fournier, L. A. McDonnell, MALDI imaging and profiling MS of higher mass proteins from tissue. *J. Am. Soc. Mass Spectrom.* **2010**, *21*, 1922.
- [9] B. K. Seyfried, J. Siekmann, O. Belgacem, R. J. Wenzel, P. L. Turecek, G. Allmaier. MALDI linear TOF mass spectrometry of PEGylated (glyco)proteins. *J. Mass Spectrom.* **2010**, *45*, 612.
- [10] H. Kraus. Cryogenic detectors and their application to mass spectrometry. *Int. J. Mass Spectrom.* **2002**, *215*, 45.
- [11] D. W. Koppenaal, C. J. Barinaga, M. B. Denton, R. P. Sperline, G. M. Hieftje, G. D. Schilling, F. J. Andrade, J. H. Barnes, I. V. Iv. MS detectors. *Anal. Chem.* **2005**, *77*, 418 A.
- [12] M. Frank, S. E. Labov, G. Westmacott, W. H. Benner. Energy-sensitive cryogenic detectors for high-mass biomolecule mass spectrometry. *Mass Spectrom. Rev.* **1999**, *18*, 155.
- [13] M. Frank. Mass spectrometry with cryogenic detectors. *Nuclear Instrum. Methods Phys. Res. Sect. A* **2000**, *444*, 375.
- [14] R. J. Wenzel, U. Matter, L. Schultheis, R. Zenobi. Analysis of megadalton ions using cryodetection MALDI time-of-flight mass spectrometry. *Anal. Chem.* **2005**, *77*, 4329.
- [15] M. Heller, D. Stalder, E. Schlappritzi, G. Hayn, U. Matter, A. Haeberli. Mass spectrometry-based analytical tools for the molecular protein characterization of human plasma lipoproteins. *Proteomics* **2005**, *5*, 2619.
- [16] N. Zen, K. Suzuki, S. Shiki, M. Ohkubo. Niobium superconducting strip line detectors (SSLD) for time-of-flight mass spectrometry (TOF-MS). *Physica C: Superconductivity* **2009**, *469*, 1684.
- [17] A. Casaburi, N. Zen, K. Suzuki, M. Ejrnaes, S. Pagano, R. Cristiano, M. Ohkubo. Subnanosecond time response of large-area superconducting stripline detectors for keV molecular ions. *Appl. Phys. Lett.* **2009**, *94*.
- [18] J. Park, H. Qin, M. Scalf, R. T. Hilger, M. S. Westphall, L. M. Smith, R. H. Blick. A mechanical nanomembrane detector for time-of-flight mass spectrometry. *Nano Lett.* **2011**, *11*, 3681.
- [19] L. A. McDonnell, R. M. A. Heeren. Mass spectrometry imaging. *Mass Spectrom. Rev.* **2007**, *26*, 606.
- [20] J. H. Jungmann, R. M. A. Heeren. Emerging technologies in mass spectrometry imaging. *J. Proteomics* **2012**, *75*, 5077.
- [21] D. W. Chandler, P. L. Houston. Two-dimensional imaging of state-selected photodissociation products detected by multiphoton ionization. *J. Chem. Phys.* **1987**, *87*, 3.
- [22] A. Eppink, D. H. Parker. Velocity map imaging of ions and electrons using electrostatic lenses: Application in photoelectron and photofragment ion imaging of molecular oxygen. *Rev. Sci. Instrum.* **1997**, *68*, 3477.
- [23] S. L. Luxembourg, T. H. Mize, L. A. McDonnell, R. M. A. Heeren. High-spatial resolution mass spectrometric imaging of peptide and protein distributions on a surface. *Anal. Chem.* **2004**, *76*, 5339.
- [24] C. R. Gebhardt, T. P. Rakitzis, P. C. Samartzis, V. Ladopoulos, T. N. Kitsopoulos. Slice imaging: A new approach to ion imaging and velocity mapping. *Rev. Sci. Instrum.* **2001**, *72*, 3848.
- [25] V. Papadakis, T. N. Kitsopoulos. Slice imaging and velocity mapping using a single field. *Rev. Sci. Instrum.* **2006**, *77*.
- [26] D. Townsend, M. P. Minitti, A. G. Suits. Direct current slice imaging. *Rev. Sci. Instrum.* **2003**, *74*, 2530.
- [27] V. Mergel, R. Dorner, J. Ullrich, O. Jagutzki, S. Lencinas, S. Nuttgens, L. Spielberger, M. Unverzagt, C. L. Cocke, R. E. Olson, M. Schulz, U. Buck, H. Schmidtbocking. He²⁺ on He – state-selective, scattering-angle-dependent capture cross-sections measured by cold target recoil ion momentum spectroscopy (COLTRIMS). *Nuclear Instrum. Methods Phys. Res. Sect. B* **1995**, *98*, 593.
- [28] J. Ullrich, R. Moshhammer, R. Dorner, O. Jagutzki, V. Mergel, H. SchmidtBocking, L. Spielberger. Recoil-ion momentum spectroscopy. *J. Phys. B Atomic Molecular and Optical Physics* **1997**, *30*, 2917.
- [29] R. Dorner, V. Mergel, O. Jagutzki, L. Spielberger, J. Ullrich, R. Moshhammer, H. Schmidt-Bocking. Cold Target Recoil Ion Momentum Spectroscopy: a 'momentum microscope' to view atomic collision dynamics. *Phys. Rep. Rev. Sect. Phys. Lett.* **2000**, *330*, 95.
- [30] J. A. Panitz, E. W. Müller, S. Brooks McLane. The atom-probe field ion microscope. *Rev. Sci. Instrum.* **1968**, *39*.
- [31] M. Leisch. Atom-probe field-ion microscopy. *Mikrochim. Acta* **1992**, *107*, 95.
- [32] R. Bellazzini, G. Spandre, M. Minuti, A. Brez, L. Baldini, L. Latronico, N. Omodei, C. Sgro, J. Bregeon, M. Razzano, M. Pinchera, A. Tremsin, J. McPhate, J. V. Vallerga, O. Siegmund. Single photon imaging at ultra-high resolution. *Nuclear Instrum. Methods Phys. Res. Sect. A* **2008**, *591*, 125.
- [33] J. Vallerga, J. McPhate, A. Tremsin, O. Siegmund. High-resolution UV, alpha and neutron imaging with the

- Timepix CMOS readout. *Nuclear Instrum. Methods Phys. Res. Sect. A* **2008**, 591, 151.
- [34] O. Siegmund, A. Tremsin, J. Vallerger, J. McPhate. Micro-channel plate cross-strip detectors with high spatial and temporal resolution. *Nuclear Instrum. Methods Phys. Res. Sect. A* **2009**, 610, 118.
- [35] H. G. Boettger, C. E. Giffin, D. D. Norris, in *Multichannel Image Detectors*, vol. 102, American Chemical Society, **1979**, p. 291.
- [36] B. Hedfjaell, R. Ryhage. Electrooptical ion detector for capillary column gas chromatography/negative ion mass spectrometry. *Anal. Chem.* **1979**, 51, 1687.
- [37] B. Hedfjaell, R. Ryhage. Electrooptical ion detector for gas chromatography/mass spectrometry. *Anal. Chem.* **1981**, 53, 1641.
- [38] J. S. Cottrell, S. Evans. The application of a multichannel electro-optical detection system to the analysis of large molecules by FAB mass spectrometry. *Rapid Commun. Mass Spectrom.* **1987**, 1, 1.
- [39] C. E. Giffin, H. G. Boettger, D. D. Norris, An electro-optical detector for focal plane mass spectrometers, *Int. J. Mass Spectrom. Ion Phys.* **1974**, 15, 437.
- [40] J. G. Aase, J. K. Burchill, D. J. Knudsen, J. P. Hackett, B. Moffat. Spatial resolution and relative brightness of a microchannel plate detector system with P20 and P43 phosphor screens. *Opt. Eng.* **2011**, 50, 064001.
- [41] M. Lampton, C. W. Carlson. Low-distortion resistive anodes for two-dimensional position-sensitive MCP systems. *Rev. Sci. Instrum.* **1979**, 50, 1093.
- [42] R. W. Odom, B. K. Furman, C. A. Evans, C. E. Bryson, W. A. Petersen, M. A. Kelly, D. H. Wayne. Quantitative image acquisition system for ion microscopy based on the resistive anode encoder. *Anal. Chem.* **1983**, 55, 574.
- [43] R. H. Bringham, R. J. Bleiler, P. J. McNitt, D. A. Reed, R. H. Fleming. Characterization of 2 resistive anode encoder position-sensitive detectors for use in ion microscopy. *Rev. Sci. Instrum.* **1993**, 64, 420.
- [44] A. Oelsner, O. Schmidt, M. Schicketanz, M. Klais, G. Schonhense, V. Mergel, O. Jagutzki, H. Schmidt-Bocking. Microspectroscopy and imaging using a delay line detector in time-of-flight photoemission microscopy. *Rev. Sci. Instrum.* **2001**, 72, 3968.
- [45] O. Jagutzki, V. Mergel, K. Ullmann-Pfleger, L. Spielberger, U. Spillmann, R. Dorner, H. Schmidt-Bocking. A broad-application microchannel-plate detector system for advanced particle or photon detection tasks: large area imaging, precise multi-hit timing information and high detection rate. *Nuclear Instrum. Methods Phys. Res. Sect. A* **2002**, 477, 244.
- [46] O. Jagutzki, A. Cerezo, A. Czasch, R. Dorner, M. Hattass, M. Huang, V. Mergel, U. Spillmann, K. Ullmann-Pfleger, T. Weber, H. Schmidt-Bocking, G. D. W. Smith. Multiple hit readout of a microchannel plate detector with a three-layer delay-line anode. *IEEE Trans. Nucl. Sci.* **2002**, 49, 2477.
- [47] O. H. W. Siegmund, M. Lampton, J. Bixier, S. Chakrabarti, J. Vallerger, S. Bowyer, R. F. Malina. Wedge and strip image readout systems for photon-counting detectors in space astronomy. *J. Opt. Soc. Am. A* **1986**, 3, 2139.
- [48] O.H.W. Siegmund, S. Clothier, J. Thornton, J. Lemen, R. Harper, I. M. Mason, J. L. Culhane. Application of the wedge and strip anode to position sensing with microchannel plates and proportional counters. *IEEE Trans. Nucl. Sci.* **1983**, NS-30, 503.
- [49] J. S. Lapington, A. D. Smith, D. M. Walton, H. E. Schwarz. Microchannel plate pore size limited imaging with ultra-thin wedge and strip anodes. *IEEE Trans. Nucl. Sci.* **1987**, NS-34, 431.
- [50] J. S. Lapington, R. Kessel, D. M. Walton. Spatial-resolution limitations of microchannel plate conductive charge division readout devices. *Nuclear Instrum. Methods Phys. Res. Sect. A* **1988**, 273, 663.
- [51] O. Siegmund, A. Tremsin, J. Vallerger, J. McPhate. Micro-channel plate cross-strip detectors with high spatial and temporal resolution. *Nuclear Instrum. Methods Phys. Res. Sect. A* **2009**, 610, 118.
- [52] O. H. W. Siegmund, A. S. Tremsin, J. V. Vallerger, J. Hull. Cross strip imaging anodes for microchannel plate detectors. *IEEE Trans. Nuc. Sci.* **2001**, 48, 430.
- [53] O. H. W. Siegmund, A. S. Tremsin, J. V. Vallerger, R. Abiad, J. Hull. High resolution cross strip anodes for photon counting detectors. *Nuclear Instrum. Methods Phys. Res. Sect. A* **2003**, 504, 177.
- [54] L. A. Klerk, N. P. Lockyer, A. Kharchenko, L. MacAleese, P. Y. W. Dankers, J. C. Vickerman, R. M. A. Heeren. C_{60}^{+} secondary ion microscopy using a delay line detector. *Anal. Chem.* **2010**, 82, 801.
- [55] M. Froesch, S. L. Luxembourg, D. Verheijde, R. M. A. Heeren. Mass spectrometry imaging using a delay-line detector. *Eur. J. Mass Spectrom.* **2010**, 16, 35.
- [56] U. Vohrer, C. Blomfield, S. Page, A. Roberts. Quantitative XPS imaging—new possibilities with the delay-line detector. *Appl. Surf. Sci.* **2005**, 252, 61.
- [57] G. A. van Riessen, S. M. Thurgate. Auger photoelectron coincidence spectroscopy: simplifying complexity. *Surf. Interface Anal.* **2006**, 38, 691.
- [58] O. Ghafur, W. Siu, P. Johnsson, M. F. Kling, M. Drescher, M. J. J. Vrakking. A velocity map imaging detector with an integrated gas injection system. *Rev. Sci. Instrum.* **2009**, 80, 033110.
- [59] G. Gademann, Y. Huismans, A. Gijsbertsen, J. Jungmann, J. Visschers, M. J. J. Vrakking. Velocity map imaging using an in-vacuum pixel detector. *Rev. Sci. Instrum.* **2009**, 80, 103105.
- [60] J. H. Jungmann, A. Gijsbertsen, J. Visser, J. Visschers, R. M. A. Heeren, M. J. J. Vrakking. A new imaging method for understanding chemical dynamics: Efficient slice imaging using an in-vacuum pixel detector. *Rev. Sci. Instrum.* **2010**, 81, 103112.
- [61] J. H. Jungmann, L. MacAleese, R. Buijs, F. Giskes, A. de Snaijer, J. Visser, J. Visschers, M. J. J. Vrakking, R. M. A. Heeren. Fast, high resolution mass spectrometry imaging using a Medipix pixelated detector. *J. Am. Soc. Mass Spectrom.* **2010**, 21, 2023.
- [62] J. H. Jungmann, L. MacAleese, J. Visser, M. J. J. Vrakking, R. M. A. Heeren. High dynamic range bio-molecular ion microscopy with the Timepix detector. *Anal. Chem.* **2011**, 83, 7888.
- [63] C. Bamberger, U. Renz, A. Bamberger. Digital imaging mass spectrometry. *J. Am. Soc. Mass Spectrom.* **2011**, 22, 1079.
- [64] A. Nomerotski, S. Adigun-Boaye, M. Brouard, E. Campbell, A. Clark, J. Crooks, J. J. John, A. J. Johnsen, C. Slater, R. Turchetta, C. Vallance, E. Wilman, W. H. Yuen. Pixel imaging mass spectrometry with fast silicon detectors. *Nuclear Instrum. Methods Phys. Res. Sect. A* **2011**, 633, S243.
- [65] J. V. Vallerger, O. H. W. Siegmund. $2\text{ K} \times 2\text{ K}$ resolution element photon counting MCP sensor with >200 kHz event rate capability. *Nuclear Instrum. Methods Phys. Res. Sect. A* **2000**, 442, 159.
- [66] O. H. W. Siegmund, J. V. Vallerger, A. Martin, B. Feller, M. Arif, D. S. Hussey, D. L. Jacobson. A high spatial resolution event counting neutron detector using micro-channel plates and cross delay line readout. *Nuclear Instrum. Methods Phys. Res. Sect. A* **2007**, 579, 188.
- [67] A. S. Tremsin, G. V. Lebedev, O. H. W. Siegmund, J. V. Vallerger, J. S. Hull, J. B. McPhate, C. Jozwiak, Y. Chen, J. H. Guo, Z. X. Shen, Z. Hussain. High spatial and

- temporal resolution photon/electron counting detector for synchrotron radiation research. *Nuclear Instrum. Methods Phys. Res. Sect. A* **2007**, 580, 853.
- [68] A. S. Tremsin, O. H. W. Siegmund, J. S. Hull, J. V. Vallerga, J. B. McPhate, J. Soderstrom, J. W. Chiou, J. H. Guo, Z. Hussain. High resolution photon counting detection system for advanced inelastic X-ray scattering studies. *IEEE Trans. Nucl. Sci.* **2007**, 54, 706.
- [69] J. Vallerga, A. Tremsin, R. Raffanti, O. Siegmund. Centroiding algorithms for high speed crossed-strip readout of microchannel plate detectors. *Nuclear Instrum. Methods Phys. Res. Sect. A* **2011**, 633, S255.
- [70] H. Spieler. *Semiconductor Detector Systems*, Oxford University Press, Oxford, **2005**.
- [71] J. Vallerga, J. McPhate, A. Tremsin, O. Siegmund. High-resolution UV, alpha and neutron imaging with the Timepix CMOS readout. *Nuclear Instrum. Methods Phys. Res. Sect. A* **2008**, 591, 151.
- [72] A. S. Tremsin, J. V. Vallerga, J. B. McPhate, O. H. W. Siegmund, W. B. Feller, L. Crow, R. G. Cooper. On the possibility to image thermal and cold neutron with sub-15 μ m spatial resolution. *Nuclear Instrum. Methods Phys. Res. Sect. A* **2008**, 592, 374.
- [73] O. H. Siegmund, J. V. Vallerga, A. S. Tremsin, J. McPhate, B. Feller. High spatial resolution neutron sensing microchannel plate detectors. *Nuclear Instrum. Methods Phys. Res. Sect. A* **2007**, 576, 178.
- [74] G. E. Smith. The invention and early history of the CCD. *Nuclear Instrum. Methods Phys. Res. Sect. A* **2009**, 607, 1.
- [75] W. S. Boyle, G. E. Smith. Nobel Prize 2009, Royal Swedish Academy of Sciences. Press release: http://www.nobel-prize.org/nobel_prizes/physics/laureates/2009/press.html (06 October **2009**).
- [76] T. O. Teledyne. DALSA, Canada, **2012**. Available: http://www.teledynedalsa.com/corp/markets/ccd_vs_cmos.aspx.
- [77] D. Litwiller. CCD vs. CMOS: Facts and fiction. *Photonics Spectra* January **2001**.
- [78] N. Wermes. Pixel detectors for particle physics and imaging applications. *Nuclear Instrum. Methods Phys. Res. Sect. A* **2003**, 512, 277.
- [79] N. Wermes. Pixel detectors for tracking and their spin-off in imaging applications. *Nuclear Instrum. Methods Phys. Res. Sect. A* **2005**, 541, 150.
- [80] H. Krüger. 2D Detectors for particle physics and for imaging applications. *Nuclear Instrum. Methods Phys. Res. Sect. A* **2005**, 551, 1.
- [81] X. Llopart, M.; C. Campbell, R. Dinapoli, D. San Segundo, E. Pernigotti. Medipix2, a 64 k pixel readout chip with 55micron square elements working in single photon counting mode, *IEEE Trans. Nucl. Sci.* **2002**, 49, 2279.
- [82] M. Locker, P. Fischer, S. Krimmel, H. Kruger, M. Lindner, K. Nakazawa, T. Takahashi, N. Wermes. Single photon counting X-ray imaging with Si and CdTe single chip pixel detectors and multichip pixel modules. *Ieee Trans. Nucl. Sci.* **2004**, 51, 1717.
- [83] P. Pangaud, S. Basolo, N. Boudet, J.-F. Berar, B. Chantepie, P. Delpierre, B. Dinkespiler, S. Hustache, M. Menouni, C. Morel. XPAD3: A new photon counting chip for X-ray CT-scanner. *Nuclear Instrum. Methods Phys. Res. Sect. A* **2007**, 571, 321.
- [84] S. Basolo, J. F. Bérar, N. Boudet, P. Breugnon, B. Chantepie, J. C. Clémens, P. Delpierre, B. Dinkespiler, S. Hustache, K. Medjoubi, M. Ménouni, C. Morel, P. Pangaud, E. Vigeolas. A 20 kpixels CdTe photon-counting imager using XPAD chip. *Nuclear Instrum. Methods Phys. Res. Sect. A* **2008**, 589, 268.
- [85] N. Boudet, J. F. Berar, L. Blanquart, P. Breugon, B. Caillot, J. C. Clemens, I. Koudobine, P. Delpierre, C. Mouget, R. Potheau, I. Valin. XPAD: a hybrid pixel detector for X-ray diffraction and diffusion. *Nuclear Instrum. Methods Phys. Res. Sect. A* **2003**, 510, 41.
- [86] B. Henrich, A. Bergamaschi, C. Broennimann, R. Dinapoli, E. F. Eikenberry, I. Johnson, M. Kobas, P. Kraft, A. Mozzanica, B. Schmitt. PILATUS: A single photon counting pixel detector for X-ray applications. *Nuclear Instrum. Methods Phys. Res. Sect. A* **2009**, 607, 247.
- [87] R. Dinapoli, A. Bergamaschi, B. Henrich, R. Horisberger, I. Johnson, A. Mozzanica, E. Schmid, B. Schmitt, A. Schreiber, X. Shi, G. Theidel. EIGER: Next generation single photon counting detector for X-ray applications. *Nuclear Instrum. Methods Phys. Res. Sect. A* **2012**, in press.
- [88] R. Ballabriga, M. Campbell, E. Heijne, X. Llopart, L. Tlustos, W. Wong. Medipix3: A 64 k pixel detector readout chip working in single photon counting mode with improved spectrometric performance. *Nuclear Instrum. Methods Phys. Res. Sect. A* **2011**, 633, S15.
- [89] X. Llopart, M. Campbell. First test measurements of a 64 k pixel readout chip working in single photon counting mode. *Nuclear Instrum. Methods Phys. Res. Sect. A* **2003**, 509, 157.
- [90] M. Campbell. 10 years of the Medipix2 collaboration. *Nuclear Instrum. Methods Phys. Res. Sect. A* **2012**, in press.
- [91] A. Nomerotski, S. Adigun-Boaye, M. Brouard, E. Campbell, A. Clark, J. Crooks, J. J. John, A. J. Johnsen, C. Slater, R. Turchetta, C. Vallance, E. Wilman, W. H. Yuen. Pixel imaging mass spectrometry with fast silicon detectors. *Nuclear Instrum. Methods Phys. Res. Sect. A* **2012**, in press.
- [92] X. Llopart, R. Ballabriga, M. Campbell, L. Tlustos, W. Wong. Timepix, a 65 k programmable pixel readout chip for arrival time, energy and/or photon counting measurements. *Nuclear Instrum. Methods Phys. Res. Sect. A* **2007**, 581, 485.
- [93] G. Mazza, A. Ceccucci, E. Cortina, A. Cotta Ramusino, G. Dellacasa, M. Fiorini, S. Garbolino, P. Jarron, J. Kaplon, A. Kluge, F. Marchetto, E. Martin, S. Martoiu, M. Noy, F. Petrucci, P. Riedler, A. Rivetti, S. Tiuraniemi. The NA62 Gigatracker pixel detector system. *Nuclear Instrum. Methods Phys. Res. Sect. A* **2010**, 617, 558.
- [94] M. Fiorini, V. Carassiti, A. Ceccucci, E. Cortina, A. Cotta Ramusino, G. Dellacasa, P. Jarron, J. Kaplon, A. Kluge, F. Marchetto, E. Martin, S. Martoiu, G. Mazza, M. Noy, F. Petrucci, P. Riedler, A. Rivetti, S. Tiuraniemi. The NA62 Gigatracker: Detector properties and pixel read-out architectures. *Nuclear Instrum. Methods Phys. Res. Sect. A* **2010**, 624, 314.
- [95] M. Fiorini, V. Carassiti, A. Ceccucci, E. Cortina, A. Cotta Ramusino, G. Dellacasa, S. Garbolino, P. Jarron, J. Kaplon, A. Kluge, A. Mapelli, F. Marchetto, E. Martin, S. Martoiu, G. Mazza, M. Morel, M. Noy, G. Nuessle, F. Petrucci, P. Riedler, G. Aglieri Rinella, A. Rivetti, S. Tiuraniemi. The Gigatracker: An ultra-fast and low-mass silicon pixel detector for the NA62 experiment. *Nuclear Instrum. Methods Phys. Res. Sect. A* **2012**, in press.
- [96] A. Kluge, G. Aglieri Rinella, V. Carassiti, A. Ceccucci, E. Cortina, J. Daguin, G. Dellacasa, M. Fiorini, S. Garbolino, P. Jarron, J. Kaplon, F. Marchetto, E. Martin, A. Mapelli, G. Mazza, M. Morel, M. Noy, G. Nuessle, P. Petagna, L. Perktold, A. Cotta Ramusino, P. Riedler, A. Rivetti, R. Wheadon. NA62 Gigatracker. *PoS VERTEX* **2010**, 040.
- [97] G. Aglieri Rinella, M. Noy, M. Fiorini, P. Jarron, J. Kaplon, A. Kluge, E. Martin, M. Morel, L. Perktold, P. Riedler. Characterisation Of The NA62 GigaTracker End Of Column Readout ASIC. *Proc. Topical Workshop on Electronics for Particle Physics* 2010, JINST **2010**, submitted.
- [98] J.-P. Jansson, A. Maentyniemi, J. Kostmovaara. A CMOS time-to-digital converter with better than 10 ps single-shot precision. *IEEE J. Solid-State Circuits* **2006**, 41, 1286.
- [99] J. Richardson, R. Walker, L. Grant, D. Stoppa, F. Borghetti, E. Charbon, M. Gersbach, R. K. Henderson. A 32x32 50 ps Resolution 10 bit Time to Digital Converter Array in

- 130 nm CMOS for Time Correlated Imaging. *IEEE 2009 Custom Integrated Circuits Conference* **2009**.
- [100] D. Stoppa, F. Borghetti, J. Richardson, R. Walker, R. K. Henderson, M. Gersbach, E. Charbon. Ultra Compact and Low-Power TDC and TAC Architectures for Highly-Parallel Implementation in Time-Resolved Image Sensors. *2011 International Workshop on ADC Modelling, Testing And Data Converter Analysis and Design and IEEE 2011 ADC Forum*, **2011**.
- [101] E. Charbon. Single-photon detection – Evolving CMOS technology for high-performance. *OPN Optics Photonics News* **2011**, 14.
- [102] Y. Maruyama, E. Charbon. A time-gated 128×128 CMOS SPAD array for on-chip fluorescence detection, in *Proc. Intl. Image Sensor Workshop (IISW)*, **2011**.
- [103] Medipix Collaboration. Available: www.cern.ch/medipix.
- [104] M. Campbell, E. H. M. Heijne, G. Meddeler, E. Pernigotti, W. Snoeys. A readout chip for a 64×64 pixel matrix with 15-bit single photon counting. *IEEE Trans. Nucl. Sci.* **1998**, 45, 751.
- [105] X. L. Llopart. Design and characterization of 64 K pixels chips working in single photon processing mode. *PhD thesis*, Mid Sweden University, Sweden, **2007**.
- [106] M. Chmeissani, B. Mikulec. Performance limits of a single photon counting pixel system. *Nuclear Instrum. Methods Phys. Res. Sect. A* **2001**, 460, 81.
- [107] M. G. Bisogni, M. Boscardin, D. Bulajic, G. F. Della Betta, P. Delogu, M. E. Fantacci, M. Novelli, C. Piemonte, M. Quattrocchi, V. Rosso, A. Stefanini, N. Zorzi. Performance of an imaging system based on silicon pixel detectors of different thickness. *IEEE Trans. Nucl. Sci.* **2005**, 52, 1989.
- [108] B. Norlin, C. Frojdh, H. E. Nilsson, H. Graafsma, V. Vonk, C. Ponchut. Characterisation of the charge sharing in pixelated Si detectors with single-photon processing readout. *Nuclear Instrum. Methods Phys. Res. Sect. A* **2006**, 563, 133.
- [109] A. Korn, M. Firsching, G. Anton, M. Hoheisel, T. Michel. Investigation of charge carrier transport and charge sharing in X-ray semiconductor pixel detectors such as Medipix2. *Nuclear Instrum. Methods Phys. Res. Sect. A* **2007**, 576, 239.
- [110] A. A. A. Aarts, H. vander Graaf, S. vander Putten. New results on a gaseous detector using Medipix2 and Micromegas. *Nuclear Instrum. Methods Phys. Res. Sect. A* **2006**, 563, 205.
- [111] Y. Giomataris, P. Rebougeard, J. P. Robert, G. Charpak. MICROMEAS: a high-granularity position-sensitive gaseous detector for high particle-flux environments. *Nuclear Instrum. Methods Phys. Res. Sect. A* **1996**, 376, 29.
- [112] L. Tlustos. Performance and limitations of high granularity single photon processing X-ray imaging detectors. *PhD thesis*, University of Technology, Vienna, Austria, **2005**.
- [113] H. Graafsma, P. Thorander, G. Heunen, J. Morse. Wide dynamic range germanium detector for perturbation crystallography. *J. Synchrotron Radiat.* **1996**, 3, 156.
- [114] D. Pennicard, H. Graafsma. Simulated performance of high-Z detectors with Medipix3 readout. *J. Instrumentation* **2011**, 6, P06007.
- [115] Z. Vykydal, J. Visschers, D. S. Tezcan, K. De Munck, T. Borgers, W. Ruythooren, P. De Moor. The RELAXd project: Development of four-side tilable photon-counting imagers. *Nuclear Instrum. Methods Phys. Res. Sect. A* **2008**, 591, 241.
- [116] S. Spiesshoefer, Z. Rahman, G. Vangara, S. Polamreddy, S. Burkett, L. Schaper. Process integration for through-silicon vias. *J. Vac. Sci. Technol. A* **2005**, 23, 824.
- [117] T. Holy, J. Jakubek, S. Pospisil, J. Uher, D. Vavrik, Z. Vykydal. Data acquisition and processing software package for Medipix2. *Nuclear Instrum. Methods Phys. Res. Sect. A* **2006**, 563, 254.
- [118] D. Turecek, T. Holy, J. Jakubek, S. Pospisil, Z. Vykydal. Pixelman: a multi-platform data acquisition and processing software package for Medipix2, Timepix and Medipix3 detectors. *J. Instrumentation* **2011**, 6, C01046.
- [119] Z. Vykydal, J. Jakubek, S. Pospisil. USB interface for Medipix2 pixel device enabling energy and position-sensitive detection of heavy charged particles. *Nucl. Instrum. Meth. A* **2006**, 563, 112.
- [120] Z. Vykydal, J. Jakubek. USB Lite—Miniaturized readout interface for Medipix2 detector. *Nuclear Instrum. Methods Phys. Res. Sect. A* **2011**, 633, Supplement 1, S48.
- [121] V. Kraus, M. Holik, J. Jakubek, M. Kroupa, P. Soukup, Z. Vykydal. FITPix – fast interface for Timepix pixel detectors. *J. Instrumentation* **2011**, 6, C01079.
- [122] D. San Segundo Bello, M. van Beuzekom, P. Jansweijer, H. Verkooijen, J. Visschers. An interface board for the control and data acquisition of the Medipix2 chip. *Nuclear Instrum. Methods Phys. Res. Sect. A* **2003**, 509, 164.
- [123] J. Visser, B. van der Heijden, S. J. A. Weijers, R. de Vries, J. L. Visschers. A Gigabit per second read-out system for Medipix Quads. *Nuclear Instrum. Methods Phys. Res. Sect. A* **2012**, in press.
- [124] J. Vallergera, R. Raffanti, A. Tremsin, J. McPhate, O. Siegmund. MCP detector read out with a bare quad Timepix at kilohertz frame rates. *J. Instrumentation* **2011**, 6, C01049.
- [125] C. Ponchut, J. Clément, J.-M. Rigal, E. Papillon, J. Vallergera, D. LaMarra, B. Mikulec. Photon-counting X-ray imaging at kilohertz frame rates. *Nuclear Instrum. Methods Phys. Res. Sect. A* **2007**, 576, 109.
- [126] M. Maiorino, R. Martinez, G. Pellegrini, G. Blanchot, M. Chmeissani, J. Garcia, M. Lozano, C. Puigdemogles, M. Ullan. A read-out system for the Medipix2 chip capable of 500 frames per second. *Nuclear Instrum. Methods Phys. Res. Sect. A* **2006**, 563, 96.
- [127] M. P. Sinha, M. Wadsworth. Miniature focal plane mass spectrometer with 1000-pixel modified-CCD detector array for direct ion measurement. *Rev. Sci. Instrum.* **2005**, 76, 025103.
- [128] O. Hadjar, W. K. Fowler, G. Kibelka, W. C. Schnute. Preliminary demonstration of an IonCCD as an alternative pixelated anode for direct MCP readout in a compact MS-based detector. *J. Am. Soc. Mass Spectrom.* **2012**, 23, 418.
- [129] O. Hadjar, G. Johnson, J. Laskin, G. Kibelka, S. Shill, K. Kuhn, C. Cameron, S. Kassin. IonCCD™ for direct position-sensitive charged-particle detection: from electrons and keV ions to hyperthermal biomolecular ions. *J. Am. Soc. Mass Spectrom.* **2011**, 22, 612.
- [130] E. S. Wilman, S. H. Gardiner, A. Nomerotski, R. Turchetta, M. Brouard, C. Vallance. A new detector for mass spectrometry: Direct detection of low energy ions using a multi-pixel photon counter. *Rev. Sci. Instrum.* **2012**, 83, 013304.